1521-0111/94/6/1421–1434$35.00
MOLECULAR PHARMACOLOGY

https://doi.org/10.1124/mol.118.113530
Mol Pharmacol 94:1421–1434, December 2018

Modeling and Mutational Analysis of the Binding Mode for the Multimodal Antidepressant Drug Vortioxetine to the Human 5-HT_{3A} Receptor[S]

Lucy Kate Ladefoged, Lachlan Munro, Anders J. Pedersen, Sarah C. R. Lummis, Benny Bang-Andersen, Thomas Balle, Birgit Schiøtt, and Anders S. Kristensen

Interdisciplinary Nanoscience Center, Department of Chemistry, Aarhus University, Aarhus, Denmark (L.K.L., B.S.); Department of Drug Design and Pharmacology, University of Copenhagen, Copenhagen, Denmark (L.M., A.J.P., A.S.K.); Department of Biochemistry, University of Cambridge, Cambridge, United Kingdom (S.C.R.L.); Lundbeck Research, H. Lundbeck A/S, Valby, Denmark (B.B.-A.); and Sydney School of Pharmacy, Faculty of Medicine and Health, The University of Sydney, Sydney, New South Wales, Australia (T.B.)

Received July 20, 2018; accepted September 19, 2018

ABSTRACT

5-Hydroxytryptamine$_3$ (5-HT_3) receptors are ligand-gated ion channels that mediate neurotransmission by serotonin in the central nervous system. Pharmacological inhibition of 5-HT_3 receptor activity has therapeutic potential in several psychiatric diseases, including depression and anxiety. The recently approved multimodal antidepressant vortioxetine has potent inhibitory activity at 5-HT_3 receptors. Vortioxetine has an inhibitory mechanism that differs from classic 5-HT_3 receptor competitive antagonists despite being believed to bind in the same binding site. Specifically, vortioxetine shows partial agonist activity followed by persistent and insurmountable inhibition. We have investigated the binding mode of vortioxetine at the human 5-HT_{3A} receptor through computational and in vitro experiments to provide insight into the molecular mechanisms behind the unique pharmacological profile of the drug. We find that vortioxetine binds in a manner different from currently known 5-HT_{3A} orthosteric ligands. Specifically, while the binding pattern of vortioxetine mimics some aspects of both the setron class of competitive antagonists and 5-hydroxytryptamine (5-HT) with regards to interactions with residues of the aromatic box motif in the orthosteric binding site, vortioxetine also forms interactions with residues not previously described to be important for the binding of either setrons or 5-HT such as Val202 on Loop F. Our results expand the framework for understanding how orthosteric ligands drive 5-HT_3 receptor function, which is of importance for the potential future development of novel classes of 5-HT_3 receptor antagonists.

Introduction

Serotonin [5-hydroxytryptamine (5-HT)] is a neurotransmitter that via ionotropic 5-HT_3 receptors, and a range of metabotropic receptors, regulates neural activities underlying a wide spectrum of basal as well as higher brain functions, including appetite, aggression, sleep, mood, and cognition (Berger et al., 2009). 5-HT_3 receptors belong to the pentameric ligand-gated ion channel (pLGIC) superfamily together with structurally and functionally related nicotinic acetylcholine receptors, $GABA_A$ receptors, and glycine receptors (GlyRs) (Barnes et al., 2009; Lummis, 2012; Nys et al., 2013; Nemecz et al., 2016). 5-HT_3 receptor inhibitors are in current use as antiemetics and for the treatment of irritable bowel syndrome and are considered a potential therapy for anxiety-related behavior and cognitive decline in major depressive disorder and schizophrenia (Robertson et al., 1992; Thompson et al., 2006b).

Vortioxetine (Fig. 1C) is a multimodal antidepressant that acts as an inhibitor at the serotonin transporter, an agonist at 5-HT_{1A} receptors, a partial agonist at 5-HT_{1B} receptors, and an antagonist at 5-HT_{1D}, 5-HT_3, and 5-HT_7 receptors (Bang-Andersen et al., 2011; Sanchez et al., 2015). In addition to antidepressive effects, vortioxetine has been shown to improve aspects of cognitive function such as attention, processing speed, executive function, and memory (McIntyre et al., 2014, 2017; Mahableshwarkar et al., 2015), which may be linked to activity at 5-HT_3 receptors (Mørk et al., 2013; Riga et al., 2016).

The molecular understanding of vortioxetine inhibition of 5-HT_3 receptors is currently limited. Vortioxetine is suggested to bind at the orthosteric binding site in 5-HT_{3A} receptors but

B.B.-A. is an employee of H. Lundbeck A/S.

This work was supported by the Danish Council of Independent Research for Medical Sciences [Grant DFF-404-00309]; the Lundbeck Foundation [Grants 2017-1655 and 2012-12453]; and the Carlsberg Foundation. Computations were made possible through allocations at the Centre for Scientific Computing, Arhus.

https://doi.org/10.1124/mol.118.113530.

[S] This article has supplemental material available at molpharm.aspetjournals.org.

ABBREVIATIONS: 5-HT, 5-hydroxytryptamine (serotonin); 5-HTBP, 5-hydroxytryptamine binding protein; ECD, extracellular domain; GlyR, glycine receptor; HEK-293, human embryonic kidney 293; h5-HT_{3A}, human 5-hydroxytryptamine$_{3A}$; hSERT, human serotonin transporter; IFD, induced fit docking; m5-HT_{3A}, mouse 5-HT_{3A}; MD, molecular dynamics; MM-PBSA, molecular mechanics–Poisson-Boltzmann and surface area; pLGIC, pentameric ligand-gated ion channel; WT, wild type.

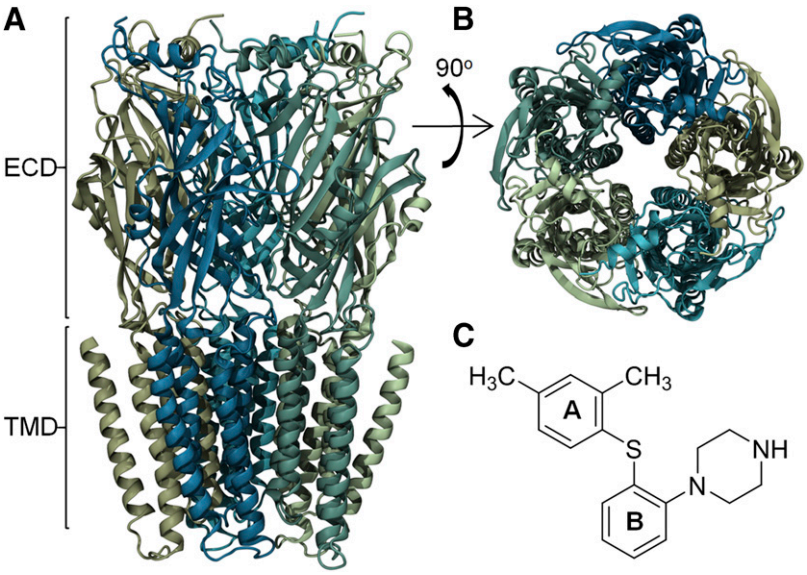

Fig. 1. Structural model of the h5-HT_{3A} receptor and chemical structure of vortioxetine. Side (A) and top (B) views of ribbon representations of the h5-HT_{3A} receptor structure created by homology modeling. Each subunit in the pentameric complex is colored individually. Brackets indicate the location of the ECD and transmembrane domain (TMD). (C) Chemical structure of vortioxetine with an indication of the A and B ring nomenclature.

differs in mechanism from other 5-HT_3 antagonists by having an initial partial agonistic response followed by an apparently insurmountable inhibition of receptor function (Bang-Andersen et al., 2011; Dale et al., 2018). Thus, vortioxetine acts as a functional antagonist under steady-state conditions, although likely through a different mechanism to that of classic competitive 5-HT_3 antagonists (collectively known as setrons). The orthosteric binding site of 5-HT_3 receptors is formed at the interface between subunits in the extracellular domain (ECD) (Nys et al., 2013; Hassaine et al., 2014; Nemecz et al., 2016). As pentamers, five potential agonist binding sites exist in the 5-HT_3 receptor. Occupancy of one or two sites appear sufficient to drive conformational ECD rearrangements that trigger channel opening and subsequent entry to a desensitized conformation (Corradi et al., 2009; Rayes et al., 2009; Hibbs and Gouaux, 2011; Andersen et al., 2013). Cryo-electron microscopy and X-ray crystal structures are available for eukaryotic pLGICs (Unwin, 2005; Hibbs and Gouaux, 2011; Unwin and Fujiyoshi, 2012; Zuber and Unwin, 2013; Althoff et al., 2014; Miller and Aricescu, 2014; Du et al., 2015; Huang et al., 2015, 2017; Morales-Perez et al., 2016), including two structures of the mouse 5-HT_{3A} (m5-HT_{3A}) receptor (Hassaine et al., 2014; Basak et al., 2018). Furthermore, AChBP (Smit et al., 2001), a soluble eukaryotic protein that forms pentamers with an overall tertiary fold similar to the ECD of pLGICs (Brejc et al., 2001), has been engineered to acquire a 5-HT_3 receptor-like ligand profile (Kesters et al., 2013). This construct, denoted as the 5-HT binding protein (5-HTBP), allows for crystallographic analysis of 5-HT_3 receptor ligand binding (Kesters et al., 2013; Price et al., 2015, 2016). Combined with computational, mutational, and biochemical analysis, structures provide insight into the molecular architecture of the 5-HT_3 receptor orthosteric binding site (Kesters et al., 2013; Hassaine et al., 2014) and ligand binding modes (Joshi et al., 2006; Moura Barbosa et al., 2010; Kesters et al., 2013; Price et al., 2015, 2016; Lochner and Thompson, 2016), and the potential conformational changes associated with ligand binding (Miller and Smart, 2010; Sander et al., 2010). From this and other work, a framework is emerging for understanding the molecular basis that underlies 5-HT_3 agonism and antagonism (Nys et al., 2013; Alix et al., 2016).

In the present study, we have studied the molecular basis of vortioxetine inhibition of human 5-HT_{3A} (h5-HT_{3A}) receptors by constructing a structural model of h5-HT_{3A}. This model is able to accurately predict the established binding mode of granisetron (Kesters et al., 2013; Ruepp et al., 2017), and was used for docking vortioxetine at the orthosteric binding site. We used pharmacological characterization of mutant receptors to identify and validate a model for vortioxetine in its bioactive conformation bound to the receptor. We find the location and conformation of vortioxetine in the binding site to be different from other known ligands, and this enables interactions with residues from both loop E and F simultaneously. Comparison with models for setron and agonist binding reveals distinct features for vortioxetine that might explain its unique inhibitory mechanism.

Materials and Methods

Materials. Chemicals were obtained from Sigma (St. Louis, MO) unless otherwise stated. Dulbecco's modified Eagle's medium, fetal bovine serum, trypsin, and penicillin-streptomycin were obtained from Invitrogen (Carlsbad, CA). DNA restriction enzymes were obtained from New England Biolabs (Ipswich, MA). Cell culture dishes were obtained from Sarstedt AG & Co (Nümbrecht, Germany), and 96-well plates were obtained from VWR (Copenhagen, Denmark). Unlabeled and tritium-labeled vortioxetine was provided by H. Lundbeck A/S (Valby, Denmark). [^{3}H]-GR65630 was obtained from Perkin Elmer (Waltham, MA). DNA sequencing was performed using GATC Biotech (Constance, Germany). The FLIPR Blue membrane potential assay kit was obtained from Molecular Devices (San Jose, CA).

Molecular Biology. cDNA encoding the h5-HT_{3A} receptor was kindly provided by Dr. Beate Niesler (University of Heidelberg). The coding sequence for h5-HT_{3A} was excised from the host vector pcDNA3.1 with *EcoR*I restriction enzyme and inserted into the combined mammalian and *Xenopus laevis* oocyte expression vector pXOON (Jespersen et al., 2002) in an *EcoR*I site in the multiple cloning site regions using T4 DNA ligase (Roche, Basel, Germany). The resulting pXOON-h5-HT_{3A} plasmid construct was confirmed by sequencing. Point mutations were generated by site-directed

mutagenesis using the QuickChange mutagenesis kit (Stratagene, La Jolla, CA). All mutant constructs were verified by DNA sequencing (Eurofins Genomics, Ebersberg, Germany).

***Xenopus laevis* Oocyte Expression.** Defoliated stage V to VI oocytes from *Xenopus laevis* were prepared as described previously (Poulsen et al., 2013) and injected with 15 ng mRNA. The care and use of *Xenopus laevis* was in strict adherence to a protocol (license 2014-15-0201-00031) approved by the Danish Veterinary and Food Administration, which is in accordance with the Guide for the Care and Use of Laboratory Animals (https://www.ncbi.nlm.nih.gov/books/NBK54050/) adopted by the U.S. National Institutes of Health. Oocytes were incubated at 18°C for 24–48 hours following injection. Recordings were made using a Warner OC725B two-electrode voltage clamp (Warner Instruments, Hamden, CT) configured as recommended by the manufacturer. For concentration-response experiments, oocytes were perfused with oocyte recording buffer (115 mM NaCl, 2 mM KCl, 5 mM HEPES, and 1.8 mM $BaCl_2$, pH 7.6) and ligands were added by whole bath application using a PC-16 valve-based perfusion controller (Bioscience Tools, Highland, CA). For fast solution switching experiments used to determine receptor desensitization rates, solutions containing saturating concentrations of agonist were applied to the oocyte using a rapid perfusion scheme with a vertical flow chamber and a volume of 400 μl and a solution flow rate of 10 ml/min (Joshi et al., 2004). This approach allowed rapid switching between control and agonist-containing solutions, which is essential to ensure resolution of desensitizing receptor currents. Solution exchange times was determined after each oocyte recording by stepping a dilute external solution across open electrode tips to measure a liquid junction current. The 10%–90% rise times for solution exchange were consistent at ~1 seconds or less. All experiments were performed at room temperature (23°C). Data acquisitions were accomplished using a Digidata 1320A analog-digital converter (Molecular Devices, San Jose, CA) interfaced with a PC running WinWCP software (available from Strathclyde Electrophysiology Software, University of Strathclyde, Glasgow, United Kingdom).

Mammalian Cell Culturing and Expression. Human embryonic kidney 293 (HEK-293) cells (American Type Culture Collection, Manassas, VA) were cultured in Dulbecco's modified Eagle's medium supplemented with 10% v/v fetal bovine serum, 100 U/ml penicillin, and 100 μg/ml streptomycin at 37°C in a humidified 5% CO_2 environment. For expression of wild-type (WT) and mutant h5-HT$_{3A}$ receptor, HEK-293 cells in suspension were transfected using TransIT DNA transfection reagent (Mirus, Madison, VA) according to the manufacturer's instructions, plated into black 96-well clear-bottom plates at a density of 30,000 cells/well, and incubated for 48 hours before use.

Membrane Potential Assay. Concentration response experiments were performed using a FlexStation 1 microplate reader (Molecular Devices, San Jose, CA) essentially as described by Price and Lummis (2005). Briefly, FLIPR blue membrane potential dye was diluted in assay buffer (denoted as Flex50 and containing 57.5 mM NaCl, 57.5 mM NMDG+, 1 mM KCl, 1 mM $MgCl_2$, 1 mM $CaCl_2$, 10 mM HEPES, and 10 mM glucose; adjusted to pH 7.4 with HCl) according to the manufacturer's instructions. Cells were incubated with 100 μl of the FLIPR blue loading solution per well at 37°C for 30 minutes. Fluorescence in each well was measured in a FlexStation 1 (Molecular Devices) scanning plate-reading fluorometer with an integrated and automated pipettor at 2-second intervals for 200 seconds. At 18 seconds, 25 μl of 5-HT solution (in Flex50 buffer, final concentration 0.01–300 μM) was added to each well. For inhibitor concentration-response experiments, the inhibitor was included in the dye loading buffer during preincubation. Experiments on the N123L mutant were performed as described previously, but using a modified assay buffer with increased NaCl concentration (denoted Flex100 and containing 115 mM NaCl, 1 mM KCl, 1 mM $MgCl_2$, 1 mM $CaCl_2$, 10 mM HEPES, and 10 mM glucose, pH 7.4) in place of Flex50 buffer to increase signal amplitude due to lower responses with this mutant receptor. Experiments on WT h5-HT$_{3A}$ receptors were performed in parallel using the Flex100 buffer, and IC_{50} values identical to those seen in the Flex50 buffer were obtained. See the Supplemental Material for additional details.

Radioligand Binding Assay. Membranes from HEK-293 cells expressing h5-HT$_{3A}$ receptors were prepared as described previously (Thompson et al., 2011). Briefly, transfected HEK-293 cells from a 10-cm dish were harvested by scraping into 1 ml ice-cold HEPES buffer (10 mM, pH 7.4) and frozen. Cells were then thawed, centrifuged at 20,000*g* for 1 minute and the pellet was resuspended in HEPES buffer. This procedure was repeated twice with a final resuspension in 2 ml HEPES buffer. For competition binding experiments, 50 μl suspensions of cell membranes were incubated in 500 μl HEPES buffer containing 0.3 nM [^{3}H]-GR65630 (equal to the K_d value for this radioligand) and varying concentrations of vortioxetine. Nonspecific binding was determined by incubation with 10 μM quipazine. For saturation binding experiments, 50 μl of cell membranes were incubated in 500 μl HEPES buffer containing increasing concentrations of [^{3}H]-vortioxetine at 4°C for 1 hour. For concentrations above 5 nM vortioxetine, [^{3}H]-vortioxetine was spiked with 2.5 nM unlabeled vortioxetine. Reactions were terminated by vacuum filtration using a Brandel (Gaithersburg, MD) cell harvester onto GF/B filters presoaked in 0.3% w/v polyethyleneimine. Radioactivity was determined by scintillation counting using a Beckman BCLS6500 instrument (Beckman, Fullerton, CA).

Pharmacological Data Analysis. All data analyses involving iterative curve fitting were performed using GraphPad Prism software (GraphPad Inc., San Diego, CA). In general, for concentration-response data for EC_{50} or IC_{50} determinations, responses were defined as the change in fluorescence or current upon agonist stimulation and calculated as peak response (R_{peak}) minus baseline fluorescence or current (R_{base}) defined as fluorescence or current immediately before agonist stimulation. For pooling of data from different experiments, we normalized responses according to the following equation:

$$\text{Normalized response} = \frac{(R_{peak} - R_{base})}{R_{max}}$$

where R_{max} is the fluorescence response recorded for application of a saturating concentration of 5-HT. For determination of IC_{50} and EC_{50} values, data were pooled among individual experiments and the composite concentration-inhibition data were analyzed by iterative curve fitting using the following equation:

$$\text{Response} = \frac{1}{(1 + 10^{(\log Y - X) \times n_H})}$$

where response is the agonist-evoked response measured at a given inhibitor concentration normalized to the response in either the absence of inhibitor (for IC_{50}) or the maximum response (for EC_{50}); Y is the concentration of inhibitor (for IC_{50}) or agonist (for EC_{50}) that produces a half-maximal inhibition or response; X is the logarithm of the concentration of the inhibitor or agonist concentration; and n_H is the Hill slope. For determination of the equilibrium dissociation constant (K_d) for vortioxetine from saturation radioligand binding experiments, specific binding data were analyzed by curve fitting according to the following equation:

$$B = \frac{(B_{max} \times [L])}{K_d + [L]}$$

where B is the bound radioligand; B_{max} is the maximum binding at equilibrium; K_d is the equilibrium dissociation constant; and $[L]$ is the free concentration of radioligand. For calculation of the inhibition constant (K_i) for vortioxetine from competition radioligand binding experiments, the Cheng-Prusoff equation (Cheng and Prusoff, 1973) was used based on the assumption that vortioxetine and the radioligand bind competitively under steady-state conditions. Unless otherwise indicated, the IC_{50} and EC_{50} values are shown with 95% confidence interval, and statistical differences were analyzed using

analysis of variance followed by a Dunnett's multiple comparisons test using the GraphPad Prism software.

Protein Modeling. The h5-HT_{3A} receptor was modeled in an inactive conformation based on several templates since no single template of a cation-selective receptor in an unambiguously inactive conformation existed at the time of modeling. Therefore, the receptor was partly modeled based on the highly homologous m5-HT_{3A} (Hassaine et al., 2014). In this structure, the pore-lining helix, M2, is in an unclear conformational state since the conformation of the backbone is similar to other open-channel receptor structures, while the conformations of the pore-lining side chains effectively close the pore (Hassaine et al., 2014). This was overcome by modeling in combination with a human $GABA_A$ receptor in an inactive conformation (Miller and Aricescu, 2014), and an antagonist-bound 5-HTBP (Kesters et al., 2013) using MODELER 9.14 (Sali and Blundell, 1993) (Supplemental Material; Supplemental Fig. 1).

Ligand Preparation. The structure of granisetron was extracted from the crystal structure of 5-HTBP (Protein Data Bank ID: 2YME), while the structure of vortioxetine was prepared as described in Andersen et al. (2015). Following assignment of bond orders and atom types in Maestro 10.1 (Schrödinger Suite 2015) (Schrodinger LLC, New York, NY), the granisetron structure was minimized and then subjected to a conformational search using the mixed torsional/low-mode sampling method, the optimized potentials for liquid simulations 2.1 force field, and an implicit water model in MacroModel 10.7 (Schrodinger Suite 2015). Then, 5000-step minimization using a conjugate gradient method followed each iteration step in the conformational search. Both ligands were modeled as having one charged amine based on available pK_a data.

Induced Fit Docking. Ligands were docked in their lowest energy conformation into each of the five substrate binding sites of h5-HT_{3A} using an induced fit docking (IFD) protocol. The protocol employed the Glide 6.4 and Prime 3.7 modules in the Schrödinger software suite (Schrödinger Suite 2015), which allows for full flexibility of both the ligand and binding site side chains (Friesner et al., 2004; Sherman et al., 2006). The binding site center was defined as the centroid of Trp178 and Ser226 in the principal subunit and Asp64 in the complementary subunit of each site. In the initial docking, Arg87 was mutated to alanine to allow room for the ligand, and a maximum of 200 poses was carried forward to the next step. A maximum of 100 ligand docking poses was reported in extra precision in the last docking step with energies less than 30 kcal/mol higher than the initial docking conformation. The resulting docking poses from each site were then combined and collectively clustered based on their in-place conformation using the Conformer Cluster script available in Maestro 10.1.

Molecular Dynamics Simulations. Simulation systems were set up and equilibrated using a coarse-grained approach before being converted into their all-atom equivalent for production run simulations. The receptor was placed in a solvated 1-palmitoyl-2-oleoyl-sn-glycero-3-phosphocholine bilayer and ionized to a 0.2 M NaCl concentration. Coarse-grained simulations were performed using the MARTINI force field (Bulacu et al., 2013; de Jong et al., 2013) and all-atom simulations using the CHARMM36 force field (Klauda et al., 2010; Best et al., 2012). The *apo* receptor was simulated in the a constant number of particles, temperature, and pressure ensemble in atomistic resolution for 10 nanoseconds, with positional restraints on C_α atoms before docking calculations. Following the docking, a representative pose from each cluster was simulated for 53.5 nanoseconds (1.5 nanoseconds of restrained equilibration, 2 nanoseconds of unrestrained preproduction equilibration, and a 50-nanosecond production run) (Supplemental Material). The analyses were performed directly after the release of the restraints to assess the stability of the binding cluster as it was found in the IFD calculations. The root-mean-square displacement of vortioxetine heavy atoms relative to their position in the first frame was monitored in each simulation as well as whether vortioxetine maintained its stabilizing interactions with the protein. See the Supplemental Material for simulation details and the parameterization of vortioxetine.

Molecular Mechanics–Poisson-Boltzmann and Surface Area Calculations. The free energy of binding was estimated using the molecular mechanics–Poisson-Boltzmann and surface area (MM-PBSA) method (Wang et al., 2001; Genheden and Ryde, 2015) as implemented in GMXPBSA 2.1 (Paissoni et al., 2015). Briefly, ligand/protein complexes were subjected to molecular dynamics (MD) simulations, and 100 frames were evenly extracted from the first 2 nanoseconds. The first 2 nanoseconds were chosen since the free energy estimate was intended as a postdocking scoring method, and not as an evaluation tool of the binding modes that vortioxetine converged into during the production runs. The first frame was extracted directly after the ligand restraints applied in the restrained equilibration phase were released, and the binding free energy is thus expected to reflect the binding mode found in the docking and not an MD-relaxed version of this binding mode. The trajectory was stripped of water, ions, and lipids, and only the ligand and the two subunits within the ECD domain that surround the ligand along with the ligand itself were included in the calculations. APBS software (Baker et al., 2001) was used to solve the Poisson-Boltzmann equation and to calculate the nonpolar contribution to the solvation energy (on the basis of the solvent accessible surface area). Gromacs 5.0.2 and the CHARMM36 force field (Klauda et al., 2010; Best et al., 2012) were used to calculate the van der Waals and Coulomb energy contributions of the free ligand and protein and the protein/ligand complex (Paissoni et al., 2015). The Poisson-Boltzmann equation was solved using a nonlinear approximation with the boundary condition defined as *sdh* and a grid spacing of 1, with the temperature set to 310 K, ion concentrations set to 0.2 M, and a protein dielectric constant of 2. Finally, the calculations were performed using the *multitrj* option in GMXPBSA (Paissoni et al., 2015) to ensure the same grid definitions in all calculations.

Results

Homology Modeling of the h5-HT_{3A} Receptor Structure. To enable computational studies of vortioxetine binding to the h5-HT_{3A} receptor, we generated a three-dimensional molecular model of h5-HT_{3A} using the existing X-ray crystal structures of pLGICs and 5-HTBP constructs as templates (see *Materials and Methods* and the Supplemental Material) (Fig. 1). Vortioxetine acts as a functional antagonist at h5-HT_{3A} by stabilizing the receptor in a closed-channel state (Bang-Andersen et al., 2011). We, therefore, chose to model the h5-HT_{3A} receptor in an inactive conformation, here defined as: 1) the channel adopting a conformation with gating residues obstructing ion passage as observed in closed-pore pLGIC structures (daCosta and Baenziger, 2013; Sauguet et al., 2015) and 2) the orthosteric binding site adopting a conformation similar to structures of antagonist-bound pLGICs and 5-HTBP constructs (Sander et al., 2010; Kesters et al., 2013). We used multiple structures as templates to build this model because a single template did not exist that represented an inactive pLGIC conformation while being sufficiently homologous to the h5-HT_{3A} receptor at the time of modeling. At the time of modeling, the closest homolog of h5-HT_{3A} for which a high-resolution structure exists is the m5-HT_{3A} receptor in the *apo* state (Hassaine et al., 2014). Human and mouse 5-HT_{3A} receptors share 86% sequence identity, and the m5-HT_{3A} structure is, therefore, in general, an excellent template for modeling of h5-HT_{3A}. However, the conformational state of the channel is unclear in the m5-HT_{3A} structure due to the low resolution of the transmembrane domain region (Hassaine et al., 2014). Therefore, to model an inactive conformational state of h5-HT_{3A}, we combined the m5-HT_{3A} structure with a structure of the human $GABA_A$ receptor

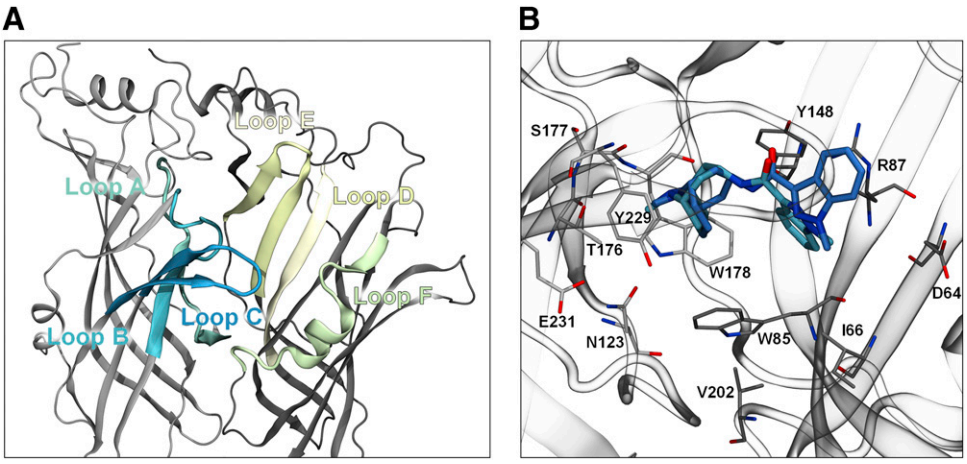

Fig. 2. Granisetron docking in the orthosteric binding site of the model h5-HT$_{3A}$ receptor structure. (A) Ribbon representation of the orthosteric binding site in the h5-HT$_{3A}$ receptor model at the subunit interface, which is formed by loops A–C in the principal subunit and loops D–F in the complementary subunit. (B) Structure of granisetron (cyan) docked in the h5-HT$_{3A}$ receptor model overlayed with the experimentally determined structure of granisetron in complex with 5-HTBP (blue) (Protein Data Bank ID: 2YME). Key principal and complimentary subunit residues are colored in white and gray, respectively. Residue numberings refer to the h5-HT$_{3A}$ sequence.

(see *Materials and Methods* and the Supplemental Material), which unambiguously is in a closed-pore conformation (Miller and Aricescu, 2014). The intracellular domain formed by the 114-residue loops between the M3 and M4 membrane-spanning domains from each subunit is not resolved in the m5-HT$_{3A}$ structure. Therefore, we did not model the intracellular domain and instead replaced the M3/M4 loop in each h5-HT$_{3A}$ subunit with a three amino acid artificial linker sequence (Supplemental Material). Finally, the conformation of the ECD loop regions that form the orthosteric binding sites were modeled using the reported X-ray crystal structure of granisetron-bound 5-HTBP (Kesters et al., 2013). The resulting h5-HT$_{3A}$ model is shown in Fig. 1, A and B. The orthosteric binding sites are located at the interfaces between subunits and formed by residues located in loops A–C on one subunit (denoted as the principal subunit) and loops D–F on the neighboring subunit (denoted as the complementary subunit) (Fig. 2A). In our model, loop C adopts an open conformation similar to the conformation observed for antagonist-bound ECD structures such as 5-HTBP in complex with setrons (Kesters et al., 2013; Price et al., 2016) as well as other antagonist-bound AChBP structures (Sander et al., 2010). Outside the binding site regions the Cys-loop is in direct contact with the M2/M3 loop through hydrophobic interactions, which is a configuration predicted to be important for allosteric communication of conformational changes between the ECD and transmembrane domain (Jha et al., 2007). The narrowest diameter of the channel pore is 2.7 Å, which is in between the pore diameters of the template GABA$_A$ and m5-HT$_{3A}$ receptor structures and is too narrow to allow ion passage (Yang, 1990; Mähler and Persson, 2012). The pore-lining residues all point into the channel pore, and the selectivity filter (Glu272) and hydrophobic gate (Leu282) (Barnes et al., 2009) are closed.

Computational Analysis of Ligand Binding to h5-HT$_{3A}$. We initially evaluated the h5-HT$_{3A}$ receptor model by docking granisetron into the orthosteric site using an IFD protocol (see *Materials and Methods*) and compared the resulting ligand-docking models with the existing structure of 5-HTBP in complex with granisetron. The resulting largest binding cluster of granisetron in the h5-HT$_{3A}$ model overlapped well with the binding mode observed in the 5-HTBP/granisetron structure (Protein Data Bank ID: 2YME, Fig. 2B), thus suggesting that our h5-HT$_{3A}$ model and docking approach is suitable for exploration of potential bioactive binding modes in the orthosteric site. Since the conformation of the orthosteric binding site in our h5-HT$_{3A}$ model is based on an antagonist-bound template, the binding site should be able to reproduce the granisetron binding mode found in a crystal structure of 5-HTBP (Kesters et al., 2013). We then docked vortioxetine into this validated model. We performed docking calculations in all five binding sites to improve the sampling of binding modes since each binding site is slightly different as no symmetry constraints were imposed during the modeling process. In total, 263 poses of vortioxetine were obtained from the five IFD calculations and clustered collectively according to their in-place conformation (see *Materials and Methods*). Among these, we dismissed all clusters with average extra precision Gscores higher than −10 kcal/mol and/or clusters containing less than six poses. The extra precision Gscore is an empirical scoring function that seeks to estimate the ligand/protein binding affinity (Friesner et al., 2006). Six clusters remained and were considered as representing the potential bioactive binding mode (C2, C6, C8, C11, C13, and C30) (Table 1). A representative orientation of vortioxetine in each of these six clusters is shown in Fig. 3. Among these, the orientation and binding site interactions of vortioxetine differ in several aspects. First, different interaction partners are observed for the charged nitrogen in the piperazine ring. In cluster C2, the charged nitrogen forms hydrogen bonds to the backbone carbonyls of Ser177 and Trp178 on loop B in addition to a cation/π interaction with Trp178. In cluster C6, the nitrogen is observed to form a salt bridge with Glu231 (loop C), whereas in clusters C8, C11, and C13, the nitrogen displays cation/π interactions with Trp178 (loop B) and Tyr229 (loop C) and hydrogen bonding to Thr176 (loop B). Finally, cluster C30 shows that the nitrogen atom in the piperazine ring is placed in the complementary subunit of the binding site where it forms a salt bridge to Asp64. Second, in all clusters one of the two aromatic rings in vortioxetine is located in the same subpocket at the back of the binding site in which one of the aromatic rings of vortioxetine is sandwiched between Tyr148 (loop E) and Trp85 (loop D) with further supporting interactions provided by Trp178 (loop B). In clusters C2, C6, and C8, the dimethylphenyl ring (phenyl A, Fig. 1C) is located in this subpocket, whereas in clusters C11, C13, and C30, it is the central phenyl (phenyl B, Fig. 1C); π/π stacking of either

TABLE 1
Results from the IFD calculations of vortioxetine into the orthosteric binding site of h5-HT_{3A}

Cluster	n^a	Average Emodel[b]	Average Gscore[b]	Average IFD score[b]
C2	24	−62.6 ± 7.1	−10.3 ± 0.9	−3139.0 ± 1.4
C6	23	−66.9 ± 10.1	−11.5 ± 1.1	3141.3 ± 1.6
C8	62	−68.4 ± 6.6	−10.3 ± 1.0	−3139.0 ± 1.4
C11	40	−64.1 ± 6.7	−10.4 ± 1.3	−3139.4 ± 1.8
C13	8	−64.1 ± 6.7	−10.4 ± 1.3	−3139.4 ± 1.8
C30	39	−70.3 ± 8.7	−10.7 ± 1.8	−3140.0 ± 2.0
Outliers	67			

[a]Number of poses within a cluster.
[b]Average Emodel, XP Gscore, and IFD scores are reported in kilocalories per mole. Data represent mean ± S.D.

phenyl of vortioxetine to at least one of the three aromatic residues within this subpocket is observed in almost all docking poses. The location of the second phenyl ring of vortioxetine is less well-defined and can be found in one of three potential locations within the binding site. In clusters C2, C6, C13, and C30 the second phenyl ring is found close to loops A, B, and C and can interact with Tyr229 (loop C) and Thr176 (loop B). However, in C11 the second phenyl, in this case phenyl A, is located close to Ile66 and Val202 (loop F) of the complementary face, while in C8, phenyl B is located at the top of the binding site close to Y148 from loop E and Leu179 from loop B. It thus becomes clear that while vortioxetine forms interactions with the same aromatic residues either by cation/π, π/π, or hydrophobic interactions, the binding clusters found in the docking calculations have distinct variations.

We further evaluated the binding clusters by performing MD simulations of each binding mode to determine the general stability of each binding mode and to estimate relative free energies of binding using the MM-PBSA approach (see *Materials and Methods*). MM-PBSA is an efficient method for fast calculation of free energies of diverse molecular systems (Homeyer and Gohlke, 2012). For clusters C8 and C13, analysis of the root-mean-square displacement progression in the MD trajectories showed the ligand remaining close to its initial conformation and position for the entire simulation period (Fig. 4, C and E), suggesting these conformations represent possible stable binding modes. In contrast, the ligand changed the conformation and position early during the simulations in cluster C2, C6, C11, and C30 (Fig. 4, A, B, D, and F), at approximately 2 nanoseconds for C6, 10 nanoseconds for C2 and C11, and immediately for C30. Interestingly, for C6 and C11, the ligand converged on a conformation similar to that observed in the stable C8 and C13, respectively. C2 converged toward a unique conformation by shifting deeper into the binding site, allowing the charged amine in the piperazine ring of vortioxetine to interact with Thr176 (loop B) (Fig. 4A). Furthermore, phenyl A rotated approximately 180°. The ligand in C30 did not change conformation during the MD simulation, but its position was shifted a few ångström closer to the complementary subunit, improving electrostatic interactions with both Asp199 and Glu224 (loops F and C, respectively). We then used the MD trajectories to perform MM-PBSA calculations to estimate the free energy of binding for each cluster (see *Materials and Methods*). The calculations were performed using the first 2 nanoseconds

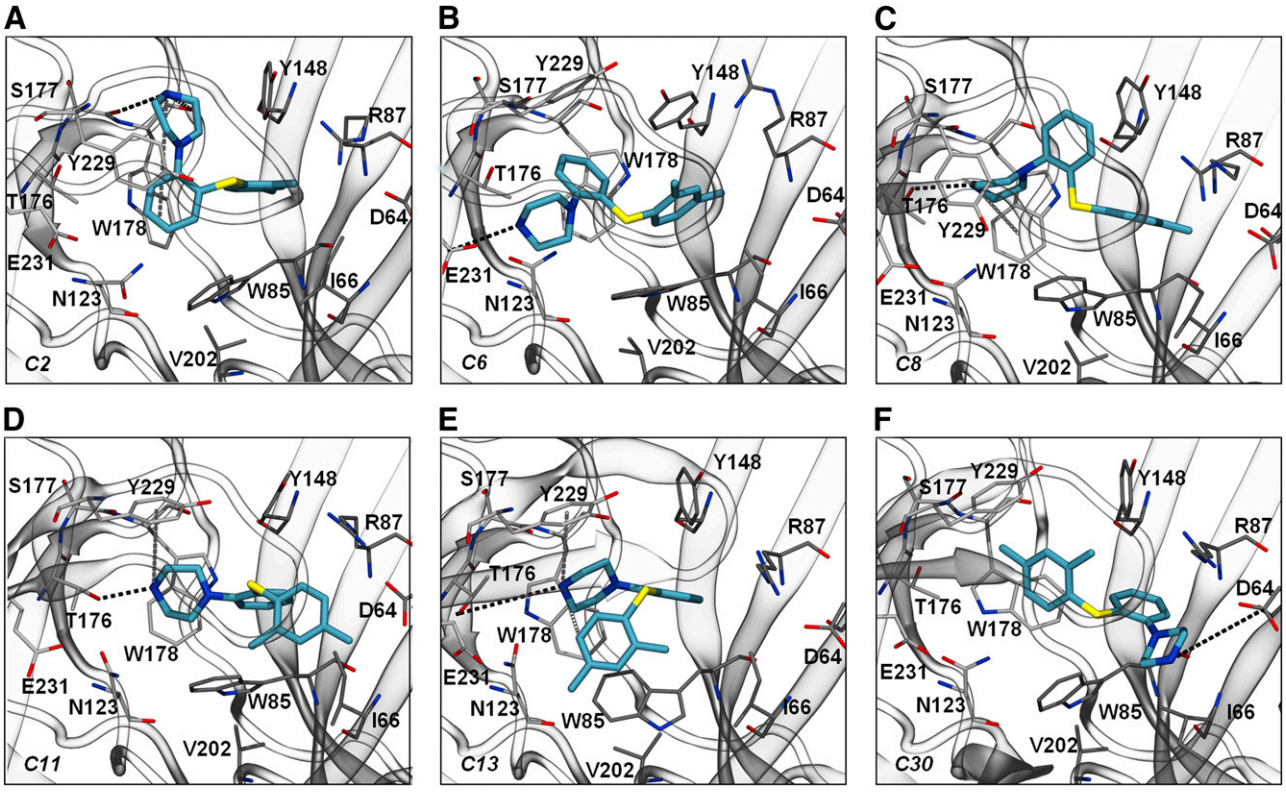

Fig. 3. Potential binding modes of vortioxetine. Representative poses of vortioxetine binding mode in the orthosteric binding site as observed in the docking clusters C2 (A), C6 (B), C8 (C), C11 (D), C13 (E), and C30 (F). Predicted interactions between the charged amine on the piperazine ring of vortioxetine and the protein are indicated with dashed lines. The key principal and complimentary subunit residues are colored in white and gray, respectively. Residue numbering refers to the h5-HT_{3A} sequence.

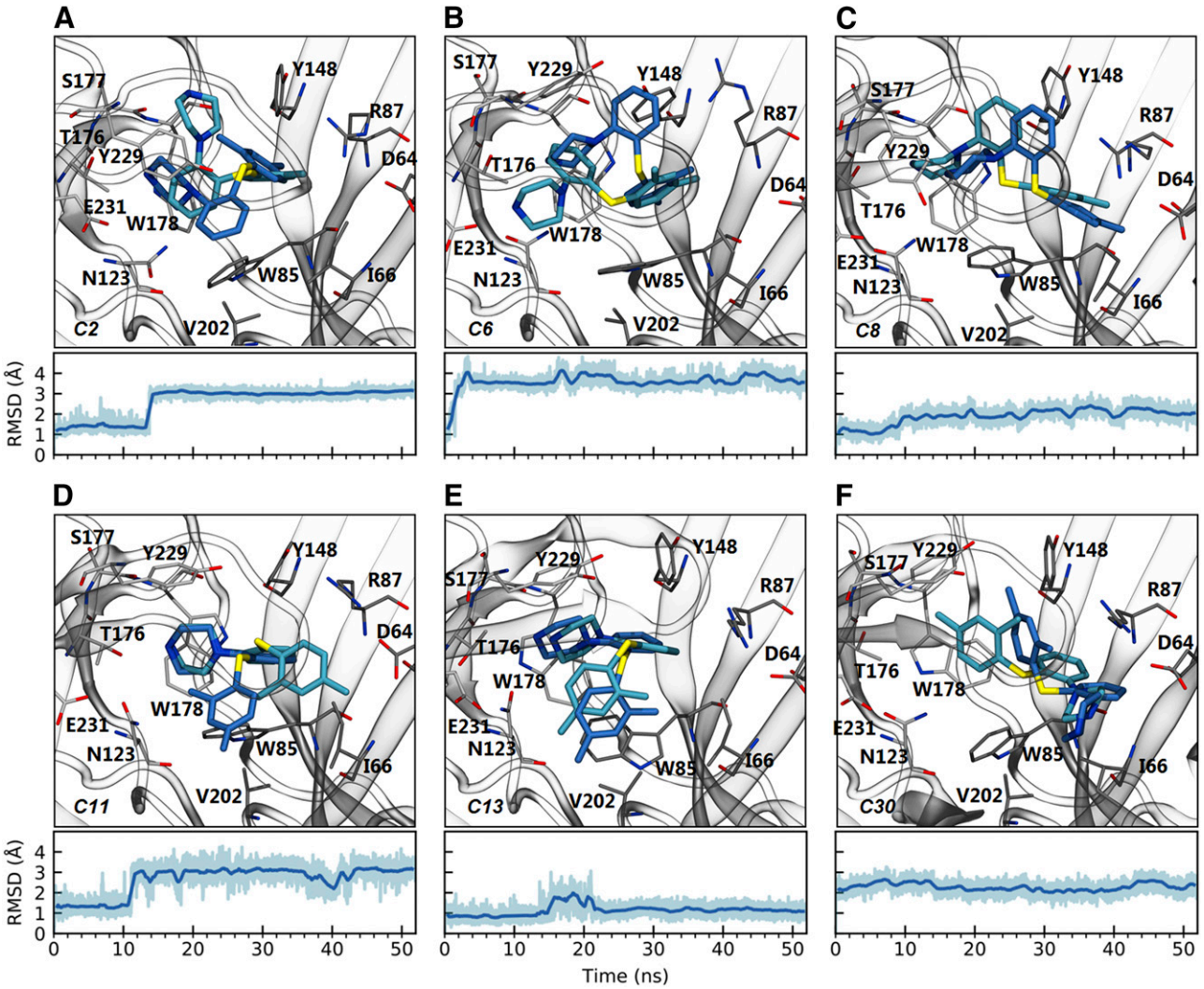

Fig. 4. Ligand stability in the orthosteric binding site during MD simulations. Overlay of vortioxetine structure before (cyan) and after (blue) 52 nanoseconds of MD simulation of vortioxetine in cluster C2 (A), C6 (B), C8 (C), C11 (D), C13 (E), and C30 (F). The structural presentation is equivalent to Fig. 3. Time course of vortioxetine movement [calculated as the root-mean-square displacement (RMSD) of vortioxetine orientation relative to initial conformation] are shown below the panels. Smoothed data are shown in dark blue, while raw data are shown in light blue.

of the MD simulations to sample only the initial binding conformations. The resulting binding energies showed clusters C8, C11, and C13 to represent the strongest binding modes (Table 2). Considered together, the results of the MD simulations and the MM-PBSA calculations suggest that C8 and C13 represent the strongest and most stable binding mode of vortioxetine in h5-HT$_{3A}$.

Characterization of Vortioxetine Activity at h5-HT$_{3A}$ Receptors. Vortioxetine properties were characterized in vitro at recombinant h5-HT$_{3A}$ receptors with the aim of establishing a methodology to determine the effects of mutation of key binding site residues on vortioxetine affinity that would allow us to challenge the binding models. Previous work with recombinant h5-HT$_{3A}$ receptors has shown vortioxetine to induce a rapidly desensitizing inward current with a peak response around 65% of that of 5-HT (Bang-Andersen et al., 2011). Using two-electrode voltage-clamp electrophysiology to measure recombinant h5-HT$_{3A}$ currents in *Xenopus* oocytes (see *Materials and Methods*), we observed similar results with saturating concentrations of vortioxetine inducing inward currents with peak response of 54% relative to 5-HT and a 7-fold faster rate of desensitization (τ_{des}) for vortioxetine (τ_{des} = 7 ± 4 seconds; n = 4) compared with 5-HT (τ_{des} = 124 ± 25 seconds for 5-HT; n = 4) (Fig. 5, B and C). Following

TABLE 2
MM-PBSA estimated binding free energies of vortioxetine for each binding cluster

Cluster	ΔG_{bind}[a]	ΔG_{bind} S.D.	$\Delta\Delta G_{bind}$[b]	$\Delta\Delta G_{bind}$ S.D.
C2	−168.8	0.8	−0.4	1.1
C6	−168.4	0.8	0	
C8	−177.8	1.1	−9.4	1.4
C11	−179.3	0.6	−10.9	1.0
C13	−184.5	0.8	−16.2	1.1
C30	−173.7	1.1	−5.4	1.3

[a]Binding free energies were calculated based on 100 frames evenly extracted from the first 2 nanoseconds of simulation as described in *Materials and Methods*, and are reported in kilocalories per mole with S.D.
[b]Relative binding free energies are reported relative to C6, which has the highest calculated binding free energy, reported in kilocalories per mole with S.D.

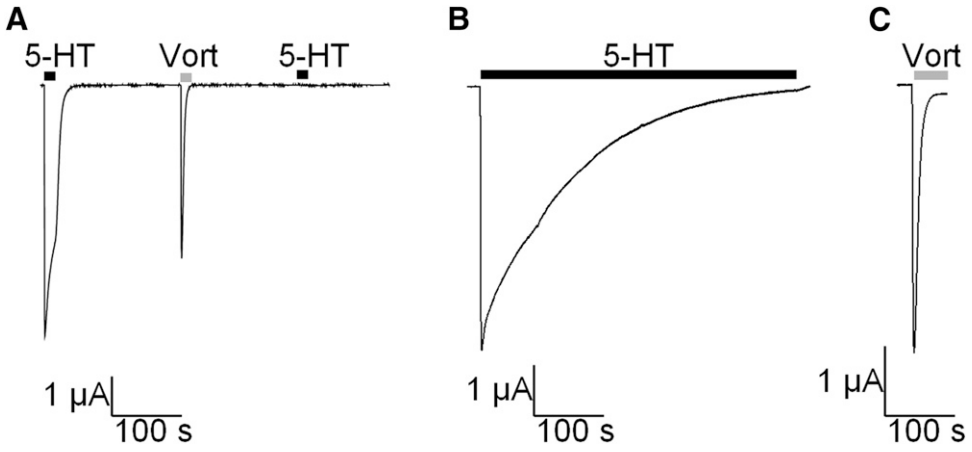

Fig. 5. Electrophysiological characterization of vortioxetine activity. (A) Current traces from a representative *Xenopus* oocyte expressing h5-HT_{3A} in response to brief 20-second applications of 10 μM 5-HT (black bar) and 10 μM vortioxetine (gray bar). Vortioxetine causes rapidly desensitizing inward currents followed by persistent inhibition. (B and C) Representative h5-HT_{3A} receptor current responses to extended application of 1 mM 5-HT (black bar; 500 seconds) and 10 μM vortioxetine (gray bar; 50 seconds). The mean ± S.E.M. for the rate of desensitization (τ_{des}) was for vortioxetine τ_{des} = 7 ± 4 seconds (S.E.M.; n = 4) and for 5-HT τ_{des} = 124 ± 25 seconds (S.E.M.; n = 4).

washout of vortioxetine, a persistent inhibition of agonist-evoked currents was observed since the subsequent application of 5-HT was unable to induce responses, consistent with what has been previously reported (Fig. 5A) (Bang-Andersen et al., 2011; Dale et al., 2018). Thus, in the two-electrode voltage-clamp assay, the persistent vortioxetine inhibition of h5-HT_{3A} prevents multiple applications of different vortioxetine concentrations to the same oocyte that are practically required for concentration-response experiments for determination of ligand potency. Thus, for a higher throughput method of determining potency of 5-HT and inhibitory potency (IC_{50}) of vortioxetine, we transiently expressed WT and mutant h5-HT_{3A} receptors in HEK-293 cells and used a microplate-based functional assay that has been used extensively for 5-HT_3 receptor pharmacological characterization (see *Materials and Methods* and the Supplemental Material) (Price and Lummis, 2005; Sullivan et al., 2006; Thompson et al., 2006a; Price et al., 2008; Lummis et al., 2011; Del Cadia et al., 2013). The assay is based on measurement of agonist-evoked changes in cell membrane potential by use of a fluorescent dye that is sensitive to the membrane field potential (Fitch et al., 2003). We evaluated the applicability of the assay by determining the concentration-response relationship for 5-HT (Fig. 5A) and concentration-inhibition relationships for two prototypical antagonists (granisetron and ondansetron) at WT h5-HT_{3A} (Supplemental Fig. 2). The membrane potential assay yielded an EC_{50} value for 5-HT of 191 nM (170–215 nM; n = 15), which is in close range of the EC_{50} value of 445 nM (255–685 nM; n = 8) determined from two-electrode voltage-clamp recordings (Fig. 6, B and C). We obtained IC_{50} values of 3.3 nM (2.7–4.1 nM; n = 6) for granisetron and 0.87 nM (0.69–1.10 nM; n = 4) for ondansetron. These values are consistent with previously reported IC_{50} values for these compounds at h5-HT_{3A} receptors (Miyake et al., 1995; Hope et al., 1996; Brady et al., 2001), thus corroborating previous assessments of the usefulness of the membrane potential assay for pharmacological characterization of recombinant 5-HT_3 receptors (Price and Lummis, 2005; Lummis and Thompson, 2013). We next used the membrane potential assay to determine the concentration-inhibition relationship of vortioxetine at 5-HT_{3A} (Fig. 6). When the cells were preincubated in increasing concentrations of vortioxetine, an IC_{50} value of 19 nM (17–21 nM; n = 20) was found (Fig. 6, E and F), which is similar to the IC_{50} value of 12 nM for inhibition of h5-HT_{3A} activity in *Xenopus* oocytes as determined by Bang-Andersen et al. (2011) and in HEK-293 cells as determined by Dale et al. (2018). We also determined vortioxetine K_i from radioligand displacement experiments using the orthosteric 5-HT_3 ligand [^{3}H]-GR65630, and obtained a K_i value of 22 nM (14–34 nM; n = 4) (Fig. 6G) and conducted saturation binding experiments using [^{3}H]-vortioxetine to determine a K_d value of 19 ± 6 nM (S.E.M.; n = 3) (Fig. 6H). These values correspond well with the IC_{50} value of vortioxetine determined in the membrane potential assay, which suggests that this assay can report affinity of vortioxetine for h5-HT_{3A} receptors. Furthermore, the highly persistent binding of vortioxetine to recombinant h5-HT_{3A} receptors observed in *Xenopus* oocytes suggests a very slow dissociation rate, i.e., after extensive washout of vortioxetine from preincubated oocytes all further application of 5-HT does not induce any current response to 5-HT. In the membrane potential assay, which employs preincubation with vortioxetine before h5-HT_{3A} responses are evoked with 5-HT, such slow unbinding should make the IC_{50} value of vortioxetine independent of 5-HT concentration. Indeed, varying concentrations of 5-HT ranging from 1 to 300 μM generated identical IC_{50} curves (Fig. 6F). Thus, the membrane potential assay overall appears suitable for characterization of vortioxetine pharmacological properties at the h5-HT_{3A}.

Mutational Analysis of Binding Site Residues that Are Predicted Critical for Vortioxetine Potency. To determine the potential contribution of binding site residues to vortioxetine affinity, we performed site-directed mutagenesis in the h5-HT_{3A} receptor and assessed the effect of single-point mutations on vortioxetine IC_{50} using the membrane potential assay. We selected eight amino acid positions around the orthosteric binding pocket for mutational analysis (Fig. 7A). The rationale for how mutation of these residues might allow us to discriminate between potential binding modes is outlined in Table 3. In general, we substituted each position with one or more residues with different physicochemical properties from the WT residue such that the mutations could change potential interactions with vortioxetine. In total, we created 14 mutants (Table 4) that were individually expressed in HEK-293 cells and assessed them for potential effects of mutation on overall receptor activity and 5-HT EC_{50} using the membrane potential assay (see *Materials and Methods*). Four mutants (D64V, N123I, S177E, and E231I) did not show specific responses to 5-HT stimulation at concentrations up to 1 mM (Table 4). Thus,

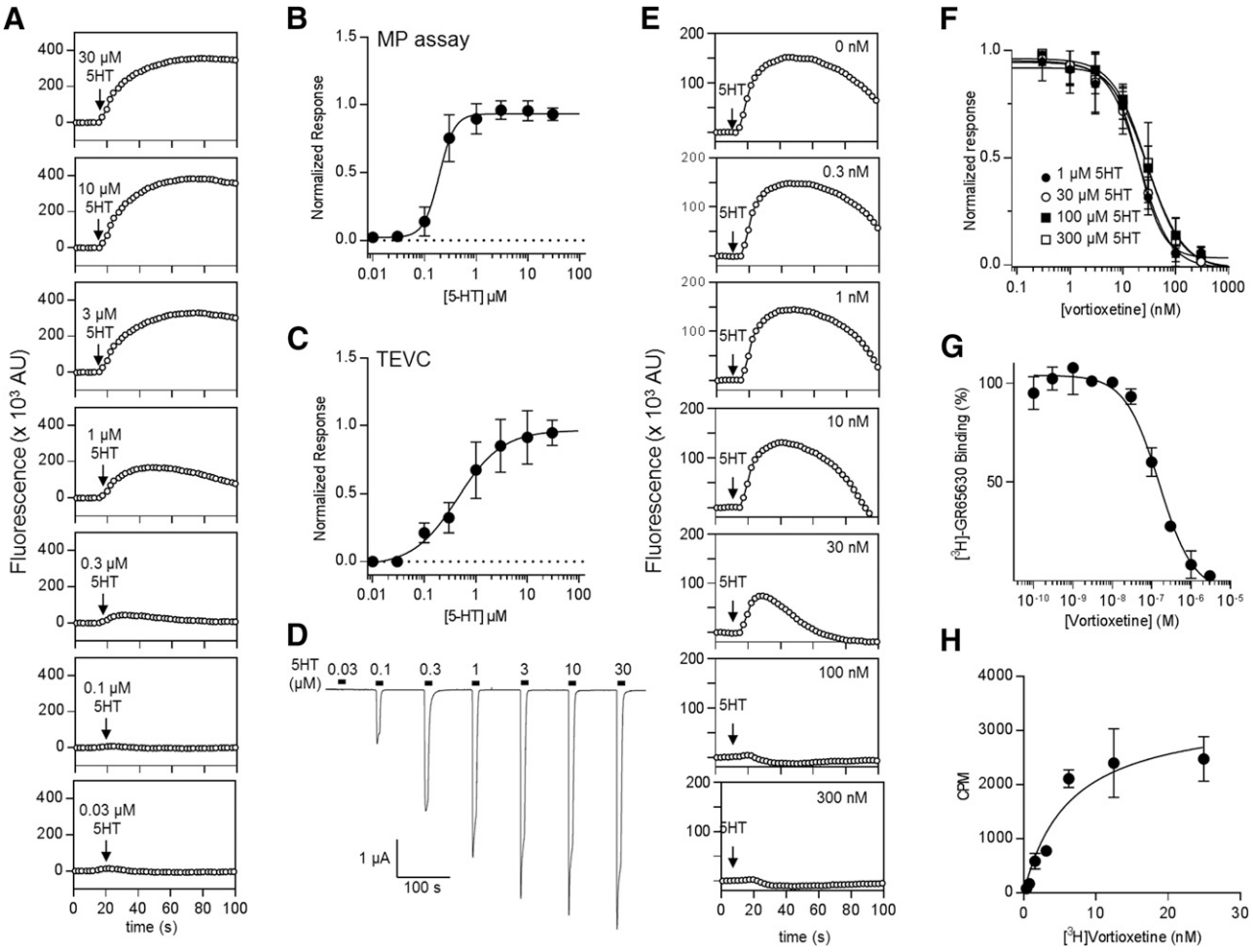

Fig. 6. Pharmacological characterization of vortioxetine in *Xenopus* oocytes and HEK-293 cells. (A) Representative trace of fluorescence responses in HEK-293 cells expressing h5-HT$_{3A}$ cells to the indicated concentration of 5-HT in micromolars using the membrane potential assay (see *Materials and Methods*). (B) Representative current responses to the indicated concentration of 5-HT (in micromolars) in *Xenopus* oocytes expressing h5-HT3$_A$ receptors at −20 mV. Concentration-response curves for 5-HT at *Xenopus* oocytes (C) and HEK-293 cells (D) expressing h5-HT$_{3A}$. Data points represent the normalized mean ± S.D. response from 5 to 10 individual experiments or oocytes for each concentration. (E) Representative trace of fluorescence responses in HEK-293 cells expressing h5-HT$_{3A}$ receptors to 30 μM 5-HT following incubation with the indicated concentration of vortioxetine using the membrane potential assay (see *Materials and Methods*). (F) Concentration-response curves for vortioxetine inhibition of h5-HT$_{3A}$ receptors at different concentrations of 5-HT. Data points represent the mean ± S.D. from three individual experiments. (G) Concentration-inhibition curve for vortioxetine displacement of [^{3}H]GR65630 binding at membranes isolated from HEK-293 cells expressing h5-HT$_{3A}$ (see *Materials and Methods*). Data points represent mean ± S.D. from at least three individual experiments. (H) Saturation analysis of [^{3}H]vortioxetine binding at cell membranes isolated from HEK-293 cells expressing h5-HT$_{3A}$.

these mutations either disrupt receptor folding and assembly, surface expression, or function. In any case, the lack of activity in the membrane potential assay prevented characterization of the potential impact of the mutations on vortioxetine pharmacology. Therefore, these functionally inactive mutants were not studied further. Previous work has reported functional mutants of Asn123 (Ala and Asp) (Thompson et al., 2005) and Ser177 (Ala and Thr) (Thompson et al., 2005) in m5-HT$_{3A}$, and Glu231 in both h5-HT$_{3A}$ and m5-HT$_{3A}$ (Gln, Asp, and Ala) (Schreiter et al., 2003; Thompson et al., 2005), whereas mutants of Asp64 have not previously been tested according to the best of our knowledge.

The remaining 10 mutants (covering five positions) were found to generate robust responses to 5-HT stimulation that allowed for determination of 5-HT EC$_{50}$ (Table 4). Increases in 5-HT EC$_{50}$ were observed for the V202A mutation and all substitutions at Thr176 and Asn123 (Table 4). These effects likely reflect that Thr176, Asn123, and V202A interact directly with 5-HT, and previous studies have observed similar shifts in 5-HT affinity upon mutations of Thr176 and Asn123 (Sullivan et al., 2006; Thompson et al., 2011). The remaining mutants displayed 5-HT EC$_{50}$ within the 2-fold range of WT. We then determined vortioxetine IC$_{50}$ at all functional binding site mutants (Fig. 7; Table 4). The mutations T176V and V202A significantly increased vortioxetine IC$_{50}$ by 5- and 11-fold, respectively, while the V202L mutation decreased the vortioxetine IC$_{50}$ by 5-fold (Fig. 8; Table 4). In contrast, all mutations of Ile66, Asn123, and Met223 produced less than 2-fold changes in vortioxetine IC$_{50}$ (Fig. 8; Table 4). These results suggest key contributions of the side chains of Thr176 and Val202 to vortioxetine binding, and no or limited contributions from Ile66, Asn123, and Met223.

Correlation between Binding Modes and Mutant Effects. We used the data set from the mutational analysis as a final assessment of the potential of each binding mode cluster to represent the bioactive binding mode of vortioxetine

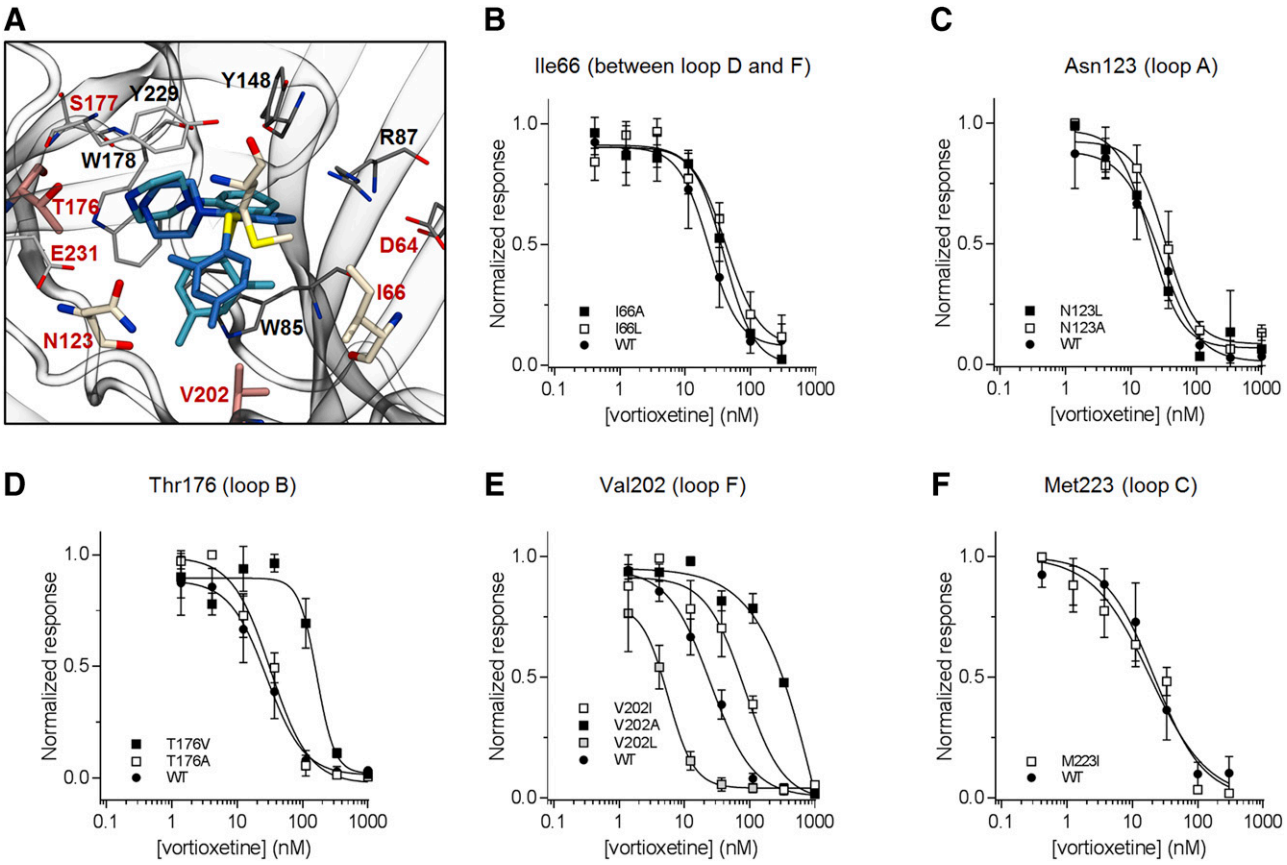

Fig. 7. Mutational analysis of vortioxetine binding. (A) Overview of key residues in the orthosteric binding site and vortioxetine orientation in the C11 (blue) and C13 (cyan) binding modes following short MD simulations. Mutated residues are labeled in red. Stick representations of residues where mutation resulted in decreased vortioxetine potency (Thr176 and Val202) are shown in pale red, and residues where mutation did not alter potency (Ile66, Asn123, and Met223) are shown in pale yellow. (B–F) Representative concentration-inhibition curves for point mutants at the indicated positions. Data points represent mean ± S.D. from at least six individual concentration-response experiments for each mutant.

in the h5-HT_{3A} receptor. The main observations that a bioactive binding mode should reconcile are: 1) gain or loss of potency upon change in bulk size of hydrophobic side chains of Val202 on loop F, 2) no or small effects upon change in bulk size of hydrophobic side chains at Ile66, and 3) 5-fold loss of potency upon removal of the side chain hydrophilicity of T176. Overall, the orientations and positions of vortioxetine in binding clusters C2, C6, and C8 do not fit well with two of these observations. First, in these binding modes the side chain of Val202 is located >6 Å from vortioxetine and displays no interactions with the ligand, which is inconsistent with the observations that vortioxetine potency is very sensitive to decrease (V202A) or subtle increase (V202L) in the bulk size of the side chain while maintaining hydrophobicity. Second, the C2, C6, and C8 binding modes predict phenyl A of vortioxetine to be located in a hydrophobic subpocket where it forms direct hydrophobic interactions with Ile66; an orientation that is inconsistent with the observed little or no effect of I66A and I66L mutations (Fig. 8).

The C11 binding mode overall fits well with the results from the mutational analysis. Vortioxetine is positioned sufficiently close to Val202 to form hydrophobic interactions with the side chain via phenyl A, which agrees with the observed effects of decreased potency upon substitution with the smaller Ala by the V202A mutation. The side chain of Ile66 is not in direct contact with vortioxetine in the stabilized conformation found via MD simulations, thus being consistent with the lack of effect of the I66A and I66L mutations. The impact of the T176V mutation on vortioxetine potency is also compatible with this binding mode since C11 predicts the presence of a hydrogen bond between the ligand piperazine secondary amine and the Thr176 side chain hydroxyl group. T176V substitutes this hydroxyl for methyl and thus disrupts any hydrogen bond capacity of this side chain, which is consistent with the observed 6-fold decrease in potency for the T176V mutant.

In C13, which was stable during the MD simulations, Val202 is making hydrophobic contacts to phenyl A and Ile66 is not in close contact with vortioxetine, which is thus consistent with the mutational results for these two residues. However, C13 predicts no ligand interaction with the side chain of Thr176 in the IFD data, in which the hydroxyl group is pointing away from the ligand. However, the MD simulations of C13 show that the side chain of Thr176 reorients such that hydrogen bonds can form between the side chain hydroxyl and the secondary amine in the piperazine ring of vortioxetine, and loss of this interaction may underlie the effect of the T176V mutation.

In C30, the side chain of Ile66 is around 4 Å from the piperazine ring, which is sufficiently distant to explain the lack of effect of Ile66 mutations that alter the bulk size of the side chain. However, Val202 is approximately 5 Å away from the ligand, which is not compatible with the substantial effects of subtle changes in the bulk size of the side chain.

TABLE 3
Rationale for mutagenesis of binding site residues and predicted impact of mutations on vortioxetine IC_{50} for binding mode clusters

Residue	Potential Binding Role of Side Chain[a]	Cluster	Mutation	Predicted Effect[a]	
				Ligand Interaction	IC_{50}
D64	γ-COOH salt bridge with piperazine NH_2	C30	V	Disruption	↑↑↑
I66	Interactions with phenyl A	C11, C13	A	Disruption	↑
I66	Interactions with phenyl A	C11, C13	L	Minor effect	Minor effect
N123	γ-NH_2 interaction with piperazine NH_2	C8	A	HB disruption	↑↑
N123	γ-NH_2 interaction with piperazine NH_2	C8	I	HB disruption	↑↑
N123	γ-NH_2 interaction with piperazine NH_2	C8	L	HB disruption	↑↑
N123	Side chain close to phenyl B	C2, C13	A	HF interaction	↓
N123	Side chain close to phenyl B	C2, C13	I	HF interaction	↓
N123	Side chain close to phenyl B	C2, C13	L	HF interaction	↓
T176	γ-OH HB interaction with piperazine NH_2	C8	A	HB disruption	↑
T176	γ-OH HB interaction with piperazine NH_2	C8	V	HB disruption	↑
T176	Transient γ-OH HB interaction with piperazine NH_2	C11, C13	A	HB disruption	Minor effect
T176	Transient γ-OH HB interaction with piperazine NH_2	C11, C13	V	HB disruption	Minor effect
S177	Side chain close to piperazine NH_2	C2	E	HB formation	↓↓
V202	Side chain distant from ligand	C2, C6, C8	A	No effect	No effect
V202	Side chain distant from ligand	C2, C6, C8	I	No effect	No effect
V202	Side chain distant from ligand	C2, C6, C8	L	No effect	No effect
V202	Side chain close to phenyl A	C11, C13	A	HF perturbation	↑
V202	Side chain close to phenyl A	C11, C13	I	HF perturbation	Minor effect
V202	Side chain close to phenyl A	C11, C13	L	HF perturbation	Minor effect
M223	Side chain close to phenyl A	C30	I	HF interaction	↓
E231	δ-COOH salt bridge with piperazine NH_2	C6	I	Disruption	↑↑↑

[a]HB, hydrogen bond; HF, hydrophobic interaction. Upwards arrow indicates predicted increase in IC_{50}, downwards arrow indicates predicted decrease in IC_{50}. Number of arrows indicates the predicted relative magnitude of the effect.

Moreover, on the opposite side of the binding pocket, the side chain of Thr176 is also more than 5 Å away from the ligand, which cannot explain the T176V effect.

In summary, the binding modes of vortioxetine observed in the C2, C6, C8, and C30 docking clusters are not compatible with the results from the mutational analysis. Combined with the results of the MD simulations and binding energy analysis, we exclude these as potential bioactive binding modes. C11 and C13 display compatibility with all mutational observations when including data from both IFD calculations and MD simulations, and thus may represent bioactive conformations of vortioxetine in vivo. During the MD simulations of C11, vortioxetine assumed a conformation that is highly similar to the conformation in C13. It is noteworthy that these binding modes then only differ by a 180° rotation of phenyl A such that the *ortho*-methyl group is pointing in opposing directions. Thus, we suggest that C11 and C13 collectively represent the binding modes of vortioxetine in the h5-HT$_{3A}$ receptor in which vortioxetine binds with some flexibility since it can bind to the receptor with the aromatic ring A in two orientations.

Discussion

Our model of the vortioxetine binding mode at the h5-HT$_{3A}$ receptor provides insight into the molecular basis for the potentially unique mode of action of vortioxetine at the 5-HT$_3$

TABLE 4
5-HT EC_{50} and vortioxetine IC_{50} values for WT and mutant h5-HT$_{3A}$ receptors

Mutant	5-HT			Vortioxetine		
	EC_{50}[a]	n[b]	Fold Change	IC_{50}[a]	n[b]	Fold Change
	μM			*nM*		
WT	0.19 [0.17; 0.21]	33		29 [25; 34]	9	
D64V	NF	3				
I66A	0.32 [0.24; 0.44]	3	1.7 [1.3; 2.3]	52 [41; 66]*	5	1.8 [1.4; 2.3]
I66L	0.27 [0.25; 0.29]	3	1.4 [1.3; 1.5]	42 [35; 50]*	5	1.4 [1.2; 1.7]
N123A	1.8 [1.5; 2.1]*	9	9.5 [8.2; 11]	47 [40; 56]*	7	1.6 [1.4; 1.9]
N123I	NF	3				
N123L	2.2 [1.4; 3.4]*	4	12 [7.6; 18]	23 [9; 57]	3	0.8 [0.3; 2.0]
T176A	2.2 [2.0; 2.5]*	6	12 [11; 13]	32 [28; 37]	5	1.1 [1.0; 1.3]
T176V	4.46 [3.83; 5.19]*	7	23 [20; 27]	146 [123; 174]*	5	5.0 [4.2; 6.0]
S177E	NF	3				
V202A	6.16 [5.53; 6.86]*	6	6.2 [5.5; 6.9]	310 [252; 386]*	8	10.7 [8.7; 13.3]
V202I	0.27 [0.24; 0.31]	4	0.27 [0.24; 0.31]	37 [30; 45]	7	1.3 [1.0; 1.6]
V202L	0.05 [0.03; 0.07]*	3	0.05 [0.03; 0.07]	5 [4; 6]*	11	0.2 [0.1; 0.2]
M223I	0.12 [0.10; 0.13]	3	0.12 [0.10; 0.13]	20 [16; 25]	5	0.7 [0.6; 0.9]
E231I	NF	3				

[a]EC_{50} and IC_{50} values were determined as described in *Materials and Methods*. Numbers in brackets denote the 95% confidence intervals.
[b]n denotes number of independent experiments.
*$P < 0.01$ vs. WT.

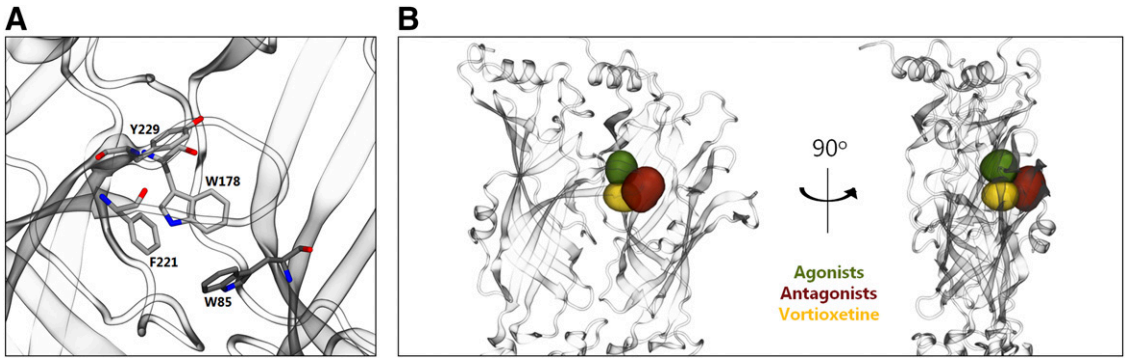

Fig. 8. Key features of the orthosteric binding site in h5-HT_{3A}. (A) Tube representation of the residues forming the aromatic box within the orthosteric binding site. All residues from the principal subunit are colored in white, while all residues from the complementary subunit are colored in gray. (B) Surface illustration of the subpockets involved in agonist (green), antagonist (red), and vortioxetine (yellow). The surrounding protein structure is shown as transparent ribbons.

receptor class. In the absence of a high-resolution structure of the h5-HT_{3A} receptor, we used homology modeling to create a structural model of the receptor in an inactive state. Recently, structures of antagonist-bound eukaryotic pLGIC receptors have become available in the form of cryo-electron microscopy structures of a zebra fish GlyR (Du et al., 2015; Huang et al., 2015). Furthermore, a crystal structure of a desensitized nicotinic acetylcholine receptor (Morales-Perez et al., 2016) and a cryo-electron microscopy structure of a preactivated m5-HT_{3A} receptor (Basak et al., 2018) have recently been published. In comparison with these structures, we find that the structures of the GlyR ECDs are very similar to our model. The single major difference is the structure of the F loop region that in our h5-HT_{3A} model and the m5-HT_{3A} crystal structure (Hassaine et al., 2014) contains a short α-helical segment, which the GlyR structures do not. However, the Val202 residue important for vortioxetine binding is located in the F loop, outside the helical segment in a region where our model and GlyR are highly similar. Additionally, our h5-HT_{3A} model is highly similar to the preactivated conformation of m5-HT_{3A} (Basak et al., 2018). These observations suggest that our model is a good representative of the inactive conformation of the h5-HT_{3A} receptor. In contrast, the conformation of h5-HT_{3A} in our model is considerably less similar to the desensitized conformation of nicotinic acetylcholine receptors (Morales-Perez et al., 2016). Since vortioxetine produces a brief agonist response in 5-HT_{3A} followed by fast and prolonged desensitization, it is possible that vortioxetine binds with strongest affinity to the desensitized state. It would, therefore, be highly relevant in future work to investigate if our proposed vortioxetine binding mode is changed in the h5$HT3_A$ model in the desensitized state. However, by the overall high degree of structural similarity to the preactivated m5-HT_{3A}, and in the ECD regions that harbor the orthosteric binding sites between our model and antagonist-bound GlyRs, we consider our present model a valid template for the ligand docking of vortioxetine.

Our ligand docking procedure yielded six possible binding modes of vortioxetine in the orthosteric binding site of the h5-HT_{3A} receptor. Following further assessment by MD simulations and binding free energy calculations, these six were narrowed down to three stable binding modes as candidates for the receptor-bound bioactive conformation of vortioxetine. We further evaluated these binding modes by mutagenesis of selected amino acid residues in the binding pocket. The observed effects of mutations on vortioxetine potency could only be fully reconciled with the highly similar C11 and C13 binding modes (Fig. 7). We, therefore, propose C11 and C13 as the bioactive binding modes. The resulting model of vortioxetine binding in the h5-HT_{3A} receptor provides a framework to understand the molecular basis for the differential mechanism of action of vortioxetine at 5-HT_{3A} compared with other 5-HT_3 orthosteric ligands. As with other pLGICs, the h5-HT_{3A} orthosteric binding pocket contains an aromatic box structural motif formed by Trp, Tyr, and Phe residues on loops A, B, C, and D (Fig. 8, Trp85, Phe221, Tyr229, and Trp178 in h5-HT_{3A}) (Beene et al., 2002a,b; Xiu et al., 2009; Thompson et al., 2010). The role of these residues is extensively studied in the 5-HT_3 receptor (Beene et al., 2002a,b, 2004; Price et al., 2008), and multiple models exist for their role in binding of setrons and agonists. Early models, and more recently also X-ray structures of 5-HTBP in complex with setrons, collectively show three main factors necessary for setron binding and effect: 1) hydrogen bonds and cation/π interactions with Trp178 in the aromatic box (Kesters et al., 2013; Lochner and Thompson, 2016; Price et al., 2016); 2) cation/π and/or π/π interactions with Tyr136, Tyr138, Tyr148, and Arg87 (Beene et al., 2004; Thompson et al., 2005, 2014; Yan and White, 2005; Joshi et al., 2006); and 3) setron occupation of a subsite beyond Arg87 near loops D and F (Fig. 8) (Kesters et al., 2013; Lochner and Thompson, 2016; Price et al., 2016). In our model, vortioxetine appears to interact with key motifs of the aromatic box in a similar manner, but also displays interactions that are distinct from setrons. A key similarity is the charged nitrogen on the piperazine ring, which is located in the center of the box and forms cation/π interactions to Trp178 and Tyr148 (Fig. 8). However, unlike setrons, vortioxetine does not interact with Tyr136, Tyr138, and Arg87 and does not occupy the subpocket beyond Arg87 (Fig. 8). Thus, the interaction pattern of vortioxetine is distinct from setrons.

In contrast to setrons, at saturating concentrations, vortioxetine also displays agonist activity at 5-HT_{3A}. As for setrons, agonist binding has been shown to require hydrogen bonding and cation/π interactions with Trp178 (Beene et al., 2002b; Price et al., 2016), suggesting this interaction to be a common denominator for ligand binding in 5-HT_3 receptors. Unlike the setrons, however, agonists interact with the 5-HTBP equivalent of Tyr148 within the complementary face and are not able

to reach as far as Arg87 in loop D (Thompson et al., 2006a). Also, agonists interact with residues from loop E as well as loop D deep within the orthosteric binding pocket (Fig. 8B). Interestingly, in our model, vortioxetine does not interact with either of these two subsites but does interact with a subsite located at loop E closer to the membrane. This unique interaction pattern of vortioxetine could underlie its distinct functional profile. In this respect, it is interesting to note that previous studies have shown Trp85 from loop D (Spier and Lummis, 2000) as well as Tyr138 and Tyr148 from loop E (Beene et al., 2004; Price and Lummis, 2004) to be necessary to produce an agonist effect, and vortioxetine interacts extensively with both Trp85 and Tyr148 in our model.

The antidepressant effect of vortioxetine involves its highly potent inhibition of the serotonin transporter (Andersen et al., 2009; Bang-Andersen et al., 2011). We have previously reported a model of vortioxetine bound in a human serotonin transporter (hSERT) (Andersen et al., 2015). Key insights into the role of functional groups of vortioxetine in binding hSERT and h5-HT_{3A} are of potential interest for future drug design of multimodal drugs targeting these serotonergic proteins. First, in both hSERT and h5-HT_{3A}, the interactions of the positively charged nitrogen in the piperazine ring mimic the interactions with the primary amine of 5-HT. Specifically, the piperazine nitrogen forms an important salt bridge to Asp98 in hSERT, and makes hydrogen bond and cation/π interactions to Thr176 and Trp178, respectively, in h5-HT_{3A}. A contrasting feature is the overall role of the two phenyl rings of vortioxetine for binding at hSERT and h5-HT_{3A}. At h5-HT_{3A}, the phenyl rings make several π/π and cation/π interactions, in particular to residues in the aromatic box, whereas in hSERT hydrophobicity of the phenyl rings rather than aromaticity is most important for binding (Andersen et al., 2015).

In summary, we have created and validated a model of the bioactive conformation of vortioxetine in the h5-HT_{3A} receptor that provides new insight into the binding of a novel multimodal serotonergic drug. The binding pattern of vortioxetine mimics some aspects of both setron and 5-HT binding but also displays binding interactions not previously described to be important for binding of either setrons or 5-HT. Since the mechanism of vortioxetine differs from classic 5-HT_{3A} orthosteric ligands with inhibitory activity such as the setrons, our results may be an important first step toward understanding the molecular basis underlying the unique properties of vortioxetine. Specifically, this will include understanding the molecular determinants for how vortioxetine binding induces a brief agonistic response followed by a rapid transition into a desensitized state from which vortioxetine has an extremely slow unbinding rate. Finally, our results provide guidance in efforts to develop multimodal drugs with tailored activity across the spectrum of serotonergic proteins.

Authorship Contributions

Participated in research design: Ladefoged, Munro, Lummis, Bang-Andersen, Balle, Schiøtt, Kristensen.

Conducted experiments: Ladefoged, Munro, Pedersen.

Contributed new reagents or analytic tools: Lummis, Bang-Andersen.

Performed data analysis: Ladefoged, Munro, Kristensen.

Wrote or contributed to the writing of the manuscript: Ladefoged, Munro, Bang-Andersen, Balle, Schiøtt, Kristensen.

References

Alix K, Khatri S, Mosier PD, Casterlow S, Yan D, Nyce HL, White MM, Schulte MK, and Dukat M (2016) Superagonist, full agonist, partial agonist, and antagonist actions of arylguanidines at 5-hydroxytryptamine-3 (5-HT_3) subunit a receptors. *ACS Chem Neurosci* **7**:1565–1574.

Althoff T, Hibbs RE, Banerjee S, and Gouaux E (2014) X-ray structures of GluCl in apo states reveal a gating mechanism of Cys-loop receptors. *Nature* **512**:333–337.

Andersen J, Kristensen AS, Bang-Andersen B, and Strømgaard K (2009) Recent advances in the understanding of the interaction of antidepressant drugs with serotonin and norepinephrine transporters. *Chem Commun (Camb)* **25**:3677–3692.

Andersen J, Ladefoged LK, Wang D, Kristensen TNB, Bang-Andersen B, Kristensen AS, Schiøtt B, and Strømgaard K (2015) Binding of the multimodal antidepressant drug vortioxetine to the human serotonin transporter. *ACS Chem Neurosci* **6**: 1892–1900.

Andersen N, Corradi J, Sine SM, and Bouzat C (2013) Stoichiometry for activation of neuronal α7 nicotinic receptors. *Proc Natl Acad Sci USA* **110**:20819–20824.

Baker NA, Sept D, Joseph S, Holst MJ, and McCammon JA (2001) Electrostatics of nanosystems: application to microtubules and the ribosome. *Proc Natl Acad Sci USA* **98**:10037–10041.

Bang-Andersen B, Ruhland T, Jørgensen M, Smith G, Frederiksen K, Jensen KG, Zhong H, Nielsen SM, Hogg S, Mørk A, et al. (2011) Discovery of 1-[2-(2,4-dimethylphenylsulfanyl)phenyl]piperazine (Lu AA21004): a novel multimodal compound for the treatment of major depressive disorder. *J Med Chem* **54**: 3206–3221.

Barnes NM, Hales TG, Lummis SC, and Peters JA (2009) The 5-HT_3 receptor—the relationship between structure and function. *Neuropharmacology* **56**:273–284.

Basak S, Gicheru Y, Samanta A, Molugu SK, Huang W, Fuente M, Hughes T, Taylor DJ, Nieman MT, Moiseenkova-Bell V, et al. (2018) Cryo-EM structure of 5-HT_{3A} receptor in its resting conformation. *Nat Commun* **9**:514.

Beene DL, Brandt GS, Lester HA, and Dougherty DA (2002a) Comparison of the cation-π interaction at the agonist binding-sites of the nicotinic-acetylcholine receptor and the 5-hydroxytryptamine-3 receptor. *Biophys J* **82**:257a.

Beene DL, Brandt GS, Zhong W, Zacharias NM, Lester HA, and Dougherty DA (2002b) Cation-π interactions in ligand recognition by serotonergic (5-HT_{3A}) and nicotinic acetylcholine receptors: the anomalous binding properties of nicotine. *Biochemistry* **41**:10262–10269.

Beene DL, Price KL, Lester HA, Dougherty DA, and Lummis SCR (2004) Tyrosine residues that control binding and gating in the 5-hydroxytryptamine$_3$ receptor revealed by unnatural amino acid mutagenesis. *J Neurosci* **24**:9097–9104.

Berger M, Gray JA, and Roth BL (2009) The expanded biology of serotonin. *Annu Rev Med* **60**:355–366.

Best RB, Zhu X, Shim J, Lopes PEM, Mittal J, Feig M, and Mackerell AD Jr (2012) Optimization of the additive CHARMM all-atom protein force field targeting improved sampling of the backbone ϕ, ψ and side-chain χ_1 and χ_2 dihedral angles. *J Chem Theory Comput* **8**:3257–3273.

Brady CA, Stanford IM, Ali I, Lin L, Williams JM, Dubin AE, Hope AG, and Barnes NM (2001) Pharmacological comparison of human homomeric 5-HT_{3A} receptors versus heteromeric 5-$HT_{3A/3B}$ receptors. *Neuropharmacology* **41**:282–284.

Brejc K, van Dijk WJ, Klaassen RV, Schuurmans M, van Der Oost J, Smit AB, and Sixma TK (2001) Crystal structure of an ACh-binding protein reveals the ligand-binding domain of nicotinic receptors. *Nature* **411**:269–276.

Bulacu M, Goga N, Zhao W, Rossi G, Monticelli L, Periole X, Tieleman DP, and Marrink SJ (2013) Improved angle potentials for coarse-grained molecular dynamics simulations. *J Chem Theory Comput* **9**:3282–3292.

Cheng Y and Prusoff WH (1973) Relationship between the inhibition constant (K_1) and the concentration of inhibitor which causes 50 per cent inhibition (I_{50}) of an enzymatic reaction. *Biochem Pharmacol* **22**:3099–3108.

Corradi J, Gumilar F, and Bouzat C (2009) Single-channel kinetic analysis for activation and desensitization of homomeric 5-HT_3A receptors. *Biophys J* **97**: 1335–1345.

daCosta CJB and Baenziger JE (2013) Gating of pentameric ligand-gated ion channels: structural insights and ambiguities. *Structure* **21**:1271–1283.

Dale E, Grunnet M, Pehrson AL, Frederiksen K, Larsen PH, Nielsen J, Stensbøl TB, Ebert B, Yin H, Lu D, et al. (2018) The multimodal antidepressant vortioxetine may facilitate pyramidal cell firing by inhibition of 5-HT_3 receptor expressing interneurons: an in vitro study in rat hippocampus slices. *Brain Res* **1689**:1–11.

de Jong DH, Singh G, Bennett WFD, Arnarez C, Wassenaar TA, Schäfer LV, Periole X, Tieleman DP, and Marrink SJ (2013) Improved parameters for the Martini coarse-grained protein force field. *J Chem Theory Comput* **9**:687–697.

Del Cadia M, De Rienzo F, Weston DA, Thompson AJ, Menziani MC, and Lummis SC (2013) Exploring a potential palonosetron allosteric binding site in the 5-HT_3 receptor. *Bioorg Med Chem* **21**:7523–7528.

Du J, Lü W, Wu S, Cheng Y, and Gouaux E (2015) Glycine receptor mechanism elucidated by electron cryo-microscopy. *Nature* **526**:224–229.

Fitch RW, Xiao Y, Kellar KJ, and Daly JW (2003) Membrane potential fluorescence: a rapid and highly sensitive assay for nicotinic receptor channel function. *Proc Natl Acad Sci USA* **100**:4909–4914.

Friesner RA, Banks JL, Murphy RB, Halgren TA, Klicic JJ, Mainz DT, Repasky MP, Knoll EH, Shelley M, Perry JK, et al. (2004) Glide: a new approach for rapid, accurate docking and scoring. 1. Method and assessment of docking accuracy. *J Med Chem* **47**:1739–1749.

Friesner RA, Murphy RB, Repasky MP, Frye LL, Greenwood JR, Halgren TA, Sanschagrin PC, and Mainz DT (2006) Extra precision glide: docking and scoring incorporating a model of hydrophobic enclosure for protein-ligand complexes. *J Med Chem* **49**:6177–6196.

Genheden S and Ryde U (2015) The MM/PBSA and MM/GBSA methods to estimate ligand-binding affinities. *Expert Opin Drug Discov* **10**:449–461.

Hassaine G, Deluz C, Grasso L, Wyss R, Tol MB, Hovius R, Graff A, Stahlberg H, Tomizaki T, Desmyter A, et al. (2014) X-ray structure of the mouse serotonin 5-HT_3 receptor. *Nature* **512**:276–281.

Hibbs RE and Gouaux E (2011) Principles of activation and permeation in an anion-selective Cys-loop receptor. *Nature* **474**:54–60.
Homeyer N and Gohlke H (2012) Free energy calculations by the molecular mechanics Poisson-Boltzmann surface area method. *Mol Inform* **31**:114–122.
Hope AG, Peters JA, Brown AM, Lambert JJ, and Blackburn TP (1996) Characterization of a human 5-hydroxytryptamine3 receptor type A (h5-HT3R-AS) subunit stably expressed in HEK 293 cells. *Br J Pharmacol* **118**:1237–1245.
Huang X, Chen H, Michelsen K, Schneider S, and Shaffer PL (2015) Crystal structure of human glycine receptor-α3 bound to antagonist strychnine. *Nature* **526**:277–280.
Huang X, Chen H, and Shaffer PL (2017) Crystal structures of human GlyRα3 bound to ivermectin. *Structure* **25**:945–950.e2.
Jespersen T, Grunnet M, Angelo K, Klaerke DA, and Olesen SP (2002) Dual-function vector for protein expression in both mammalian cells and *Xenopus laevis* oocytes. *Biotechniques* **32**:536–538, 540.
Jha A, Cadugan DJ, Purohit P, and Auerbach A (2007) Acetylcholine receptor gating at extracellular transmembrane domain interface: the Cys-loop and M2-M3 linker. *J Gen Physiol* **130**:547–558.
Joshi PR, Suryanarayanan A, Hazai E, Schulte MK, Maksay G, and Bikádi Z (2006) Interactions of granisetron with an agonist-free 5-HT_{3A} receptor model. *Biochemistry* **45**:1099–1105.
Joshi PR, Suryanarayanan A, and Schulte MK (2004) A vertical flow chamber for *Xenopus* oocyte electrophysiology and automated drug screening. *J Neurosci Methods* **132**:69–79.
Kesters D, Thompson AJ, Brams M, van Elk R, Spurny R, Geitmann M, Villalgordo JM, Guskov A, Danielson UH, Lummis SC, et al. (2013) Structural basis of ligand recognition in 5-HT_3 receptors. *EMBO Rep* **14**:49–56.
Klauda JB, Venable RM, Freites JA, O'Connor JW, Tobias DJ, Mondragon-Ramirez C, Vorobyov I, MacKerell AD Jr, and Pastor RW (2010) Update of the CHARMM all-atom additive force field for lipids: validation on six lipid types. *J Phys Chem B* **114**:7830–7843.
Lochner M and Thompson AJ (2016) The muscarinic antagonists scopolamine and atropine are competitive antagonists at 5-HT_3 receptors. *Neuropharmacology* **108**:220–228.
Lummis SC (2012) 5-HT_3 receptors. *J Biol Chem* **287**:40239–40245.
Lummis SC and Thompson AJ (2013) Agonists and antagonists induce different palonosetron dissociation rates in 5-HT_3A and 5-HT_3AB receptors. *Neuropharmacology* **73**:241–246.
Lummis SC, Thompson AJ, Bencherif M, and Lester HA (2011) Varenicline is a potent agonist of the human 5-hydroxytryptamine3 receptor. *J Pharmacol Exp Ther* **339**:125–131.
Mahableshwarkar AR, Zajecka J, Jacobson W, Chen Y, and Keefe RS (2015) A randomized, placebo-controlled, active-reference, double-blind, flexible-dose study of the efficacy of vortioxetine on cognitive function in major depressive disorder. *Neuropsychopharmacology* **40**:2025–2037.
Mähler J and Persson I (2012) A study of the hydration of the alkali metal ions in aqueous solution. *Inorg Chem* **51**:425–438.
McIntyre RS, Florea I, Tonnoir B, Loft H, Lam RW, and Christensen MC (2017) Efficacy of vortioxetine on cognitive functioning in working patients with major depressive disorder. *J Clin Psychiatry* **78**:115–121.
McIntyre RS, Lophaven S, and Olsen CK (2014) A randomized, double-blind, placebo-controlled study of vortioxetine on cognitive function in depressed adults. *Int J Neuropsychopharmacol* **17**:1557–1567.
Miller PS and Aricescu AR (2014) Crystal structure of a human $GABA_A$ receptor. *Nature* **512**:270–275.
Miller PS and Smart TG (2010) Binding, activation and modulation of Cys-loop receptors. *Trends Pharmacol Sci* **31**:161–174.
Miyake A, Mochizuki S, Takemoto Y, and Akuzawa S (1995) Molecular cloning of human 5-hydroxytryptamine3 receptor: heterogeneity in distribution and function among species. *Mol Pharmacol* **48**:407–416.
Morales-Perez CL, Noviello CM, and Hibbs RE (2016) X-ray structure of the human $\alpha4\beta2$ nicotinic receptor. *Nature* **538**:411–415.
Mørk A, Montezinho LP, Miller S, Trippodi-Murphy C, Plath N, Li Y, Gulinello M, and Sanchez C (2013) Vortioxetine (Lu AA21004), a novel multimodal antidepressant, enhances memory in rats. *Pharmacol Biochem Behav* **105**:41–50.
Moura Barbosa AJ, De Rienzo F, Ramos MJ, and Menziani MC (2010) Computational analysis of ligand recognition sites of homo- and heteropentameric 5-HT_3 receptors. *Eur J Med Chem* **45**:4746–4760.
Nemecz Á, Prevost MS, Menny A, and Corringer PJ (2016) Emerging molecular mechanisms of signal transduction in pentameric ligand-gated ion channels. *Neuron* **90**:452–470.
Nys M, Kesters D, and Ulens C (2013) Structural insights into Cys-loop receptor function and ligand recognition. *Biochem Pharmacol* **86**:1042–1053.
Paissoni C, Spiliotopoulos D, Musco G, and Spitaleri A (2015) GMXPBSA 2.1: a GROMACS tool to perform MM/PBSA and computational alanine scanning. *Comput Phys Commun* **186**:105–107.
Poulsen MH, Lucas S, Bach TB, Barslund AF, Wenzler C, Jensen CB, Kristensen AS, and Strømgaard K (2013) Structure-activity relationship studies of argiotoxins: selective and potent inhibitors of ionotropic glutamate receptors. *J Med Chem* **56**:1171–1181.
Price KL, Bower KS, Thompson AJ, Lester HA, Dougherty DA, and Lummis SCR (2008) A hydrogen bond in loop A is critical for the binding and function of the 5-HT_3 receptor. *Biochemistry* **47**:6370–6377.
Price KL, Lillestol RK, Ulens C, and Lummis SC (2015) Varenicline interactions at the 5-HT_3 receptor ligand binding site are revealed by 5-HTBP. *ACS Chem Neurosci* **6**:1151–1157.
Price KL, Lillestol RK, Ulens C, and Lummis SCR (2016) Palonosetron-5-HT_3 receptor interactions as shown by a binding protein cocrystal structure. *ACS Chem Neurosci* **7**:1641–1646.
Price KL and Lummis SC (2005) FlexStation examination of 5-HT_3 receptor function using Ca^{2+} - and membrane potential-sensitive dyes: advantages and potential problems. *J Neurosci Methods* **149**:172–177.
Price KL and Lummis SCR (2004) The role of tyrosine residues in the extracellular domain of the 5-hydroxytryptamine$_3$ receptor. *J Biol Chem* **279**:23294–23301.
Rayes D, De Rosa MJ, Sine SM, and Bouzat C (2009) Number and locations of agonist binding sites required to activate homomeric Cys-loop receptors. *J Neurosci* **29**:6022–6032.
Riga MS, Sánchez C, Celada P, and Artigas F (2016) Involvement of 5-HT_3 receptors in the action of vortioxetine in rat brain: focus on glutamatergic and GABAergic neurotransmission. *Neuropharmacology* **108**:73–81.
Robertson DW, Lacefield WB, Bloomquist W, Pfeifer W, Simon RL, and Cohen ML (1992) Zatosetron, a potent, selective, and long-acting 5HT3 receptor antagonist: synthesis and structure-activity relationships. *J Med Chem* **35**:310–319.
Ruepp MD, Wei H, Leuenberger M, Lochner M, and Thompson AJ (2017) The binding orientations of structurally-related ligands can differ; a cautionary note. *Neuropharmacology* **119**:48–61.
Sali A and Blundell TL (1993) Comparative protein modelling by satisfaction of spatial restraints. *J Mol Biol* **234**:779–815.
Sanchez C, Asin KE, and Artigas F (2015) Vortioxetine, a novel antidepressant with multimodal activity: review of preclinical and clinical data. *Pharmacol Ther* **145**:43–57.
Sander T, Bruun AT, and Balle T (2010) Docking to flexible nicotinic acetylcholine receptors: a validation study using the acetylcholine binding protein. *J Mol Graph Model* **29**:415–424.
Sauguet L, Shahsavar A, and Delarue M (2015) Crystallographic studies of pharmacological sites in pentameric ligand-gated ion channels. *Biochim Biophys Acta* **1850**:511–523.
Schreiter C, Hovius R, Costioli M, Pick H, Kellenberger S, Schild L, and Vogel H (2003) Characterization of the ligand-binding site of the serotonin 5-HT_3 receptor: the role of glutamate residues 97, 224, and 235. *J Biol Chem* **278**:22709–22716.
Sherman W, Day T, Jacobson MP, Friesner RA, and Farid R (2006) Novel procedure for modeling ligand/receptor induced fit effects. *J Med Chem* **49**:534–553.
Smit AB, Syed NI, Schaap D, van Minnen J, Klumperman J, Kits KS, Lodder H, van der Schors RC, van Elk R, Sorgedrager B, et al. (2001) A glia-derived acetylcholine-binding protein that modulates synaptic transmission. *Nature* **411**:261–268.
Spier AD and Lummis SCR (2000) The role of tryptophan residues in the 5-hydroxytryptamine$_3$ receptor ligand binding domain. *J Biol Chem* **275**:5620–5625.
Sullivan NL, Thompson AJ, Price KL, and Lummis SC (2006) Defining the roles of Asn-128, Glu-129 and Phe-130 in loop A of the 5-HT_3 receptor. *Mol Membr Biol* **23**:442–451.
Thompson AJ, Duke RK, and Lummis SC (2011) Binding sites for bilobalide, diltiazem, ginkgolide, and picrotoxinin at the 5-HT_3 receptor. *Mol Pharmacol* **80**:183–190.
Thompson AJ, Lester HA, and Lummis SCR (2010) The structural basis of function in Cys-loop receptors. *Q Rev Biophys* **43**:449–499.
Thompson AJ, Padgett CL, and Lummis SCR (2006a) Mutagenesis and molecular modeling reveal the importance of the 5-HT_3 receptor F-loop. *J Biol Chem* **281**:16576–16582.
Thompson AJ, Price KL, Reeves DC, Chan SL, Chau PL, and Lummis SCR (2005) Locating an antagonist in the 5-HT_3 receptor binding site using modeling and radioligand binding. *J Biol Chem* **280**:20476–20482.
Thompson AJ, Sullivan NL, and Lummis SC (2006b) Characterization of 5-HT_3 receptor mutations identified in schizophrenic patients. *J Mol Neurosci* **30**:273–281.
Thompson AJ, Verheij MHP, Verbeek J, Windhorst AD, de Esch IJP, and Lummis SCR (2014) The binding characteristics and orientation of a novel radioligand with distinct properties at 5-HT_3A and 5-HT_3AB receptors. *Neuropharmacology* **86**:378–388.
Unwin N (2005) Refined structure of the nicotinic acetylcholine receptor at 4 Å resolution. *J Mol Biol* **346**:967–989.
Unwin N and Fujiyoshi Y (2012) Gating movement of acetylcholine receptor caught by plunge-freezing. *J Mol Biol* **422**:617–634.
Wang J, Morin P, Wang W, and Kollman PA (2001) Use of MM-PBSA in reproducing the binding free energies to HIV-1 RT of TIBO derivatives and predicting the binding mode to HIV-1 RT of efavirenz by docking and MM-PBSA. *J Am Chem Soc* **123**:5221–5230.
Xiu X, Puskar NL, Shanata JA, Lester HA, and Dougherty DA (2009) Nicotine binding to brain receptors requires a strong cation-π interaction. *Nature* **458**:534–537.
Yan D and White MM (2005) Spatial orientation of the antagonist granisetron in the ligand-binding site of the 5-HT_3 receptor. *Mol Pharmacol* **68**:365–371.
Yang J (1990) Ion permeation through 5-hydroxytryptamine-gated channels in neuroblastoma N18 cells. *J Gen Physiol* **96**:1177–1198.
Zuber B and Unwin N (2013) Structure and superorganization of acetylcholine receptor-rapsyn complexes. *Proc Natl Acad Sci USA* **110**:10622–10627.

Address correspondence to: Birgit Schiøtt, Interdisciplinary Nanoscience Center (iNANO), Department of Chemistry, Aarhus University, Langelandsgade 140, DK-8000 Aarhus, Denmark. E-mail: birgit@chem.au.dk; or [2]Anders S. Kristensen, Department of Drug Design and Pharmacology, University of Copenhagen, Universitetsparken 2, DK-2100 Copenhagen, Denmark. E-mail: ask@sund.ku.dk